

Local-density-derived semiempirical pseudopotentials

Lin-Wang Wang and Alex Zunger

National Renewable Energy Laboratory, Golden, Colorado 80401

(Received 23 January 1995)

Transferable screened atomic pseudopotentials were developed 30 years ago in the context of the empirical pseudopotential method (EPM) by adjusting the potential to reproduce observed bulk electronic energies. While extremely useful, such potentials were not constrained to reproduce wave functions and related quantities, nor was there a systematic way to assure transferability to different crystal structures and coordination numbers. Yet, there is a significant contemporary demand for accurate screened pseudopotentials in the context of electronic structure theory of nanostructures, where local-density-approximation (LDA) approaches are both too costly and insufficiently accurate, while effective-mass band approaches are inapplicable when the structures are too small. We can now improve upon the traditional EPM by a two-step process: *First*, we invert a set of self-consistently determined screened LDA potentials for a range of bulk crystal structures and unit cell volumes, thus determining spherically-symmetric and structurally averaged atomic potentials (SLDA). These potentials reproduce the LDA band structure to better than 0.1 eV, over a range of crystal structures and cell volumes. *Second*, we adjust the SLDA to reproduce *observed* excitation energies. We find that the adjustment represents a reasonably small perturbation over the SLDA potential, so that the ensuing fitted potential still reproduces a $> 99.9\%$ overlap with the original LDA pseudowave functions despite the excitation energies being distinctly non-LDA. We apply the method to Si and CdSe in a range of crystal structures, finding excellent agreement with the *experimentally determined* band energies, optical spectra $\epsilon_2(E)$, static dielectric constants, deformation potentials, and, at the same time, *LDA-quality* wave functions.

I. INTRODUCTION

In the density functional approach,^{1,2} one solves single-particle effective Schrödinger equations with a *distinct*, self-consistently determined screening potential V_{HXC} :

$$\left\{ -\frac{1}{2}\nabla^2 + \hat{V}_{\text{ext}}(\mathbf{r}) + V_{HXC}[\rho(\mathbf{r})] \right\} \psi_i = \epsilon_i \psi_i. \quad (1)$$

Here, $\hat{V}_{\text{ext}}(\mathbf{r})$ is a fixed external (possibly pseudo) potential determining the chemical and structural identity of the system, and $\rho(\mathbf{r}) = \sum_i^{\text{occ}} |\psi_i|^2$ is the charge density of all occupied single-particle states ψ_i . The external pseudopotential $\hat{V}_{\text{ext}}(\mathbf{r})$ can be written as a sum of a nonlocal pseudopotential and a local pseudopotential³

$$\begin{aligned} \hat{V}_{\text{ext}}(\mathbf{r}) &= \hat{V}_{\text{nonlocal}}(\mathbf{r}) + V_{\text{local}}(\mathbf{r}) \\ &= \hat{V}_{\text{nonlocal}}(\mathbf{r}) + \sum_{\alpha} \sum_{\mathbf{R}_{\alpha}} v_{ps}^{(\alpha)}(|\mathbf{r} - \mathbf{R}_{\alpha}|), \end{aligned} \quad (2)$$

where α is the chemical atomic type and \mathbf{R}_{α} stands for all possible atomic positions (including those related by lattice translations) of α . Here $\sum_{\mathbf{R}_{\alpha}}$ stands for a summation over all \mathbf{R}_{α} for a given α and $v_{ps}^{(\alpha)}$ is the local part of the α th atomic pseudopotential for the unscreened ion. $V_{\text{nonlocal}}(\mathbf{r})$ is the nonlocal part of the pseudopotential which can also be represented as a sum over α and \mathbf{R}_{α} of the nonlocal parts of fixed atomic pseudopotentials. We have used V and v to denote, respectively, crystalline and atomic potentials. Much of the computational effort in

solving Eq. (1) is spent in constructing and iteratively updating the screening potential $V_{HXC}[\rho(\mathbf{r})]$ using, e.g., the local-density approximation (LDA),² in which

$$V_{HXC}[\rho(\mathbf{r})] = \int \frac{\rho(\mathbf{r}')}{|\mathbf{r} - \mathbf{r}'|} d^3\mathbf{r}' + V_X[\rho(\mathbf{r})] + V_C[\rho(\mathbf{r})]. \quad (3)$$

The first term is the interelectronic Coulomb ("Hartree") potential, and V_X and V_C are the exchange and correlation potentials,² respectively. While $\hat{V}_{\text{ext}}(\mathbf{r})$ can be constructed explicitly for each system once and for all, simply by summing over fixed *atomic* potentials as in Eq. (2), $V_{HXC}[\rho(\mathbf{r})]$ is not a linear sum over atomic quantities, and must be obtained separately for each physical system without any system-to-system transferability. Here, we will first explore the possibility of constructing from Eqs. (1)–(3) *transferable* and *fixed* (i.e., screened) spherical atomic potentials (local part only) $v^{\alpha}(r)$ such that the solutions of

$$\left\{ -\frac{1}{2}\nabla^2 + \hat{V}_{\text{nonlocal}}(\mathbf{r}) + \sum_{\alpha} \sum_{\mathbf{R}_{\alpha}} v^{(\alpha)}(|\mathbf{r} - \mathbf{R}_{\alpha}|) \right\} \tilde{\psi}_i = \tilde{\epsilon}_i \tilde{\psi}_i \quad (4)$$

reproduce with a good approximation to the solutions of the LDA Eqs. (1)–(3), i.e., $\tilde{\psi}_i$ will have large overlaps with ψ_i and $\tilde{\epsilon}_i$ will be close to ϵ_i . For simplicity, the nonlocal LDA potential $\hat{V}_{\text{nonlocal}}(\mathbf{r})$ in Eq. (4) is kept

the same as in Eqs. (1) and (2).

Our approach involves two approximations. First, while $V_{HXC}(\mathbf{r})$ of Eq. (3) can be written rigorously as a sum of *nonspherical*, atom-centered potentials, we use instead in Eq. (4) a *spherical* representation. Second, while $V_{HXC}[\rho(\mathbf{r})]$ of Eq. (3) is system dependent [through the system's $\rho(\mathbf{r})$], we will assume that $v^\alpha(r)$ of Eq. (4) are fixed atomic potentials and hence transferable from one system to the other. The combined nonspherical and nontransferability error will be examined by comparing the solutions $\{\epsilon_i, \psi_i\}$ of Eq. (1) with the solutions $\{\tilde{\epsilon}_i, \tilde{\psi}_i\}$ of Eq. (4) for a few systems covering a range of coordination numbers and volumes. At this step we have a *spherical* (S) and approximately *transferable* LDA potential $v_{SLDA}^{(\alpha)}(r)$ which we will term the "SLDA." We will show that this potential provides good approximations to the LDA results for bulk systems in that the band structures are reproduced to within better than 0.1 eV over a considerable energy range. Thus the SLDA approach, like the LDA itself, suffers from poor reproduction of the *observed* excitation energies. Therefore in the second step we will empirically adjust $v_{SLDA}^{(\alpha)}(r)$ to reproduce the *experimentally* observed excitation energies. The amounts of adjustment needed will be clear indicators of "LDA errors." It is interesting to note that relatively minor changes are required in $v_{SLDA}^{(\alpha)}(r)$ to reproduce the observed excitation energies. Thus the resulting wave functions retain a large overlap with LDA wave functions. This approach yields what we term as the "semiempirical pseudopotential method," or SEPM.

This procedure could permit simple, noniterative electronic structure calculations [via Eq. (4)] for large systems.⁴⁻⁷ This approach is analogous to the well-known "empirical pseudopotential method"^{8,9} (EPM) that has been successfully applied to many systems.¹⁰ Part of the motivation of our work, however, derives from the fact that the conventional EPM, without check, sometimes gives inaccurate wave functions.¹¹ Unlike the EPM, in which $v^{(\alpha)}(r)$ was adjusted to fit the single-particle excitation spectra with no regard to the quality of the associated wave functions and charge densities, our approach produces a large (in practice $\gtrsim 99.9\%$) overlap $\langle \tilde{\psi}_i | \psi_i \rangle$ with the LDA wave functions, while reproducing *experimental* excitation energies. Furthermore, unlike the EPM, which produces only discrete form factors and is hence suitable only for a particular crystal structure and lattice constant, we will develop a *continuous* $v_{SEPM}^{(\alpha)}(r)$ which can be used for different structures and volumes with good transferability. In essence, unlike the conventional *ab initio* LDA pseudopotential-generating programs,^{3,12} which solve the equations of an isolated *atom*, we will use the LDA equations of *periodic solids* [Eqs. (1)-(3)] to extract effective, screened solid state potentials $v^{(\alpha)}(r)$ [Eq. (4)]. This approach affords a systematic procedure for generating transferable effective potentials from bulk LDA calculations, retaining LDA-like wave functions but adjusting the potential to produce accurate excitation energies. We will illustrate the method for a covalent solid (Si) and for a more ionic case (CdSe), considering in each case a number of crystal

structures and a range of unit cell volumes, thus providing information on the transferability of these potentials.

The rest of this paper is organized as follows. Section II outlines the formalism of this method, defining also all quantities used later in figures and tables. Readers who are interested only in the theoretical aspects can read just that part of the paper. Section III applies the method outlined in Sec. II to CdSe and Si systems, analyzing various steps of the approximations and comparing many electronic properties calculated by the present method to experiment. This provides the interested readers with the detailed data needed to judge this method. Most numerical results are presented as tables and figures. The final results are given in Tables XI and XII and Figs. 6-10. Section IV compares this method with other methods and discusses the area in which this method can be used.

II. CONSTRUCTION OF SEMIEMPIRICAL PSEUDOPOTENTIALS FROM BULK LDA CALCULATIONS

A. The spherical LDA potential (SLDA)

Any periodic total potential such as $\hat{V}_{\text{ionic}} + V_{HXC}$ of Eq. (1) can be rigorously expressed as a sum over atom-centered *nonspherical* functions. For example, the *local* part of the total LDA potential [Eqs. (2) and (3)] for crystal structure σ can be written as

$$V_{LDA}^{(\sigma)}(\mathbf{r}) \equiv V_{\text{local}}^{(\sigma)}(\mathbf{r}) + V_{HXC}^{(\sigma)}(\mathbf{r}) \\ = \sum_{\alpha'} \sum_{\mathbf{R}_{\alpha',\sigma}} v_{LDA}^{(\alpha',\sigma)}(\mathbf{r} - \mathbf{R}_{\alpha',\sigma}), \quad (5)$$

where α' is the lattice atomic site, which is different from α , the chemical atomic type. One α could correspond to more than one α' (e.g., the diamondlike structure). The decomposition of Eq. (5) is not unique, and neither is the nonspherical potential $v_{LDA}^{(\alpha',\sigma)}(\mathbf{r})$. However, for symmetric decompositions, $v_{LDA}^{(\alpha',\sigma)}(\mathbf{r})$ can be expanded as

$$v_{LDA}^{(\alpha',\sigma)}(\mathbf{r}) = \sum_l v_{LDA}^{(\alpha',\sigma,l)}(|\mathbf{r}|) K_l(\hat{\mathbf{r}}), \quad (6)$$

where $K_l(\hat{\mathbf{r}})$ are the Kubic harmonics of crystal structure σ (Ref. 13) for the symmetry-allowed angular momentum l . For the diamond structure, for example, the symmetry-allowed l values are 0,3,4,... . In the following, we will introduce two simplifying approximations intended to remove the dependence of $v_{LDA}^{(\alpha',\sigma,l)}(r)$ on angular momentum l and crystal structure σ and define three errors caused by these two approximations.

1. The spherical approximation

We retain only the spherically symmetric ($l = 0$) part of Eq. (6). For structures which connect all lattice

atomic sites α' of the same chemical type α with symmetry operations (e.g., the diamondlike structure), we can define $v_{\text{SLDA}}^{(\alpha,\sigma)}(r) \equiv v_{\text{LDA}}^{(\alpha',\sigma,l=0)}(r)$. The subscript ‘‘SLDA’’ denotes ‘‘spherically approximated LDA.’’ Thus we will make the following spherical approximation of Eq. (5):

$$V_{\text{LDA}}^{(\sigma)}(\mathbf{r}) \Rightarrow V_{\text{SLDA}}^{(\sigma)}(\mathbf{r}) \equiv \sum_{\alpha} \sum_{\mathbf{R}_{\alpha,\sigma}} v_{\text{SLDA}}^{(\alpha,\sigma)}(|\mathbf{r}-\mathbf{R}_{\alpha,\sigma}|). \quad (7)$$

We define as \mathbf{G}_{σ} the reciprocal lattice vectors of structure σ with unit cell volume Ω and as $V(\mathbf{G})$ the Fourier transform of $V(\mathbf{r})$. The α th atomic structure factor of structure σ is

$$S^{(\alpha,\sigma)}(\mathbf{G}_{\sigma}) = \frac{1}{\Omega} \sum'_{\mathbf{R}_{\alpha,\sigma}} e^{i\mathbf{G}_{\sigma} \cdot \mathbf{R}_{\alpha,\sigma}}, \quad (8)$$

where $\sum'_{\mathbf{R}_{\alpha,\sigma}}$ stands for summation over $\mathbf{R}_{\alpha,\sigma}$'s within one unit cell. In this notation, the spherical approximation of Eq. (7) implies the neglect of the following nonspherical potentials:

$$\begin{aligned} \Delta V_1^{(\sigma)}(\mathbf{G}_{\sigma}) &\equiv V_{\text{LDA}}^{(\sigma)}(\mathbf{G}_{\sigma}) - V_{\text{SLDA}}^{(\sigma)}(\mathbf{G}_{\sigma}) \\ &= V_{\text{LDA}}^{(\sigma)}(\mathbf{G}_{\sigma}) - \sum_{\alpha} S^{(\alpha,\sigma)}(\mathbf{G}_{\sigma}) v_{\text{SLDA}}^{(\alpha,\sigma)}(|\mathbf{G}_{\sigma}|). \end{aligned} \quad (9)$$

This quantity $[\Delta V_1^{(\sigma)}]$ is called the error of ‘‘strictly forbidden reflection’’ due to reasons explained later.

To solve for $v_{\text{SLDA}}^{(\alpha,\sigma)}(|\mathbf{G}_{\sigma}|)$, we will first solve Eqs. (1)–(3) within the LDA (using *ab initio nonlocal* pseudopotentials) for a set of structures and unit cell volumes denoted collectively by $\{\sigma\}$, finding the self-consistent Fourier coefficients $V_{\text{LDA}}^{(\sigma)}(\mathbf{G}_{\sigma})$ of Eq. (5). We then *attempt* the equality

$$V_{\text{LDA}}^{(\sigma)}(\mathbf{G}_{\sigma}) = \sum_{\alpha} S^{(\alpha,\sigma)}(\mathbf{G}_{\sigma}) v_{\text{SLDA}}^{(\alpha,\sigma)}(|\mathbf{G}_{\sigma}|) \quad (10)$$

for each structure σ . We solve Eq (10) for each \mathbf{G}_{σ} which has a nonvanished $V_{\text{LDA}}^{(\sigma)}(\mathbf{G}_{\sigma})$ and find real valued $v_{\text{SLDA}}^{(\alpha,\sigma)}(|\mathbf{G}_{\sigma}|)$. The spherical approximation of Eq. (7) manifests itself by the fact that the solution of Eq. (10) is not always exact (or even possible), thus the error $\Delta V_1^{(\sigma)}(\mathbf{G}_{\sigma})$ in Eq. (9) is nonzero. Equation (10) can be considered as a matrix linear equation for each \mathbf{G}_{σ} , with α and real and imaginary parts as its column and row indices, respectively. Because, this matrix could be singular, the solution could be not exact (or even possible). A simple example is when $S^{(\alpha,\sigma)}(\mathbf{G}_{\sigma}) = 0$ but $V_{\text{LDA}}^{(\sigma)}(\mathbf{G}_{\sigma}) \neq 0$. These are called ‘‘forbidden reflections,’’ e.g., $\mathbf{G}_{\sigma} = \{(222), (442), (622), (644), \text{ and } (842)\}$ for the diamond lattice, $\mathbf{G}_{\sigma} = \{(004), (014), (031), \text{ and } (033)\}$ for wurtzite, and $\mathbf{G}_{\sigma} = \{(002), (004), (024), \text{ and } (114)\}$ for zinc blende. For these \mathbf{G}_{σ} values, $v_{\text{SLDA}}^{(\alpha,\sigma)}(|\mathbf{G}_{\sigma}|)$ is either approximated [when $S^{(\alpha,\sigma)}(\mathbf{G}_{\sigma}) \neq 0$, but the matrix is singular] or not calculated at all [when $S^{(\alpha,\sigma)}(\mathbf{G}_{\sigma}) =$

0]. In both cases the nonspherical error is assessed by calculating $\Delta V_1^{(\sigma)}$ of Eq. (9), and is called the error of ‘‘strictly forbidden reflections.’’

There is another kind of error. The solved $v_{\text{SLDA}}^{(\alpha,\sigma)}(|\mathbf{G}_{\sigma}|)$'s are a set of numbers corresponding to a discrete $|\mathbf{G}_{\sigma}|$ set. The plot of $v_{\text{SLDA}}^{(\alpha,\sigma)}(|\mathbf{G}_{\sigma}|)$ vs $|\mathbf{G}_{\sigma}|$ can involve some scatter, so the individual points cannot be described by a *single smooth curve* (which is needed in our search for a *r*-space continuous pseudopotential). We refer to this as scatter error. We examine its consequences by fitting the points $\{v_{\text{SLDA}}^{(\alpha,\sigma)}(|\mathbf{G}_{\sigma}|), |\mathbf{G}_{\sigma}|\}$ for a given structure σ to a parametrized form

$$u_{\text{SLDA}}^{(\alpha,\sigma)}(q) = \sum_{n=1}^{20} C_{\text{SLDA}}^{(\alpha,\sigma)}(n) e^{-(q-a_n)^2/b_n^2}. \quad (11)$$

Then, the ‘‘one structure scatter error’’ for structure σ is calculated as

$$\Delta V_2^{(\alpha,\sigma)}(\mathbf{G}_{\sigma}) = v_{\text{SLDA}}^{(\alpha,\sigma)}(|\mathbf{G}_{\sigma}|) - u_{\text{SLDA}}^{(\alpha,\sigma)}(|\mathbf{G}_{\sigma}|), \quad (12)$$

where v denotes the (numerical) solutions to Eq. (10) and u denotes the fitted value of Eq (11). The error ΔV_2 reflects the neglect of the scatter of $v_{\text{SLDA}}^{(\alpha,\sigma)}(|\mathbf{G}_{\sigma}|)$ for a single structure, which is another manifestation of the error in the spherical approximation. Combining the ‘‘strictly forbidden reflection’’ error ΔV_1 of Eq. (9) with the ‘‘one structure scatter error’’ ΔV_2 of Eq. (12), gives the total error due to the spherical approximation for a given structure σ .

2. The structural average approximation

So far, the potentials $v_{\text{SLDA}}^{(\alpha,\sigma)}$ and $u_{\text{SLDA}}^{(\alpha,\sigma)}$ depend on the crystal structure σ . We now average over a number of different structures $\{\sigma\}$. Thus, at the right hand side of Eq. (7), we perform the replacement

$$v_{\text{SLDA}}^{(\alpha,\sigma)}(r) \Rightarrow v_{\text{SLDA}}^{(\alpha)}(r) \equiv \langle v_{\text{SLDA}}^{(\alpha,\sigma)}(r) \rangle_{\sigma}, \quad (13)$$

where the angular brackets denote ‘‘structural average.’’ The corresponding error can be assessed by directly comparing the two quantities in Eq. (13). Note that the spherical approximation (Sec. II A 1) [Eq. (7)] implies specific errors $\Delta V_1^{(\alpha)} + \Delta V_2^{(\alpha)}$ for a given structure σ , while the structural averaging approximation (Sec. II A 2) [Eq. (13)] concerns the transferability error of $v_{\text{SLDA}}^{(\alpha)}(r)$ used to describe *different structures* $\{\sigma\}$.

To implement the structural average of step 2, we include in the fit of Eq. (11) *all structures* $\{\sigma\}$. The resulting curve (dropping now the superscript σ) can be written as

$$u_{\text{SLDA}}^{(\alpha)}(q) = \sum_{n=1}^{20} C_{\text{SLDA}}^{(\alpha)}(n) e^{-(q-a_n)^2/b_n^2}. \quad (14)$$

The corresponding error due to structural scatter is

$$\Delta V_3^{(\alpha,\sigma)}(\mathbf{G}_\sigma) = v_{\text{SLDA}}^{(\alpha,\sigma)}(|\mathbf{G}_\sigma|) - u_{\text{SLDA}}^{(\alpha)}(|\mathbf{G}_\sigma|). \quad (15)$$

Note that this “structure averaged scatter error” ΔV_3 differs from the “one structure scatter error” ΔV_2 [Eq. (12)] in that the former involves structural averages in the fitting of u . Consequently, the magnitude of the error ΔV_3 is larger than the magnitude of ΔV_2 : the increase reflects the error introduced by structural average.

At this stage we have a spherically symmetric and structural averaged, screened atomic LDA potential $u_{\text{SLDA}}^{(\alpha)}$; this will be called the SLDA in the following discussions. We will examine the errors ΔV_1 , ΔV_2 , and ΔV_3 defined in Eqs. (9), (12), and (15), respectively. In addition, to test the effect of the total error $\Delta V_1 + \Delta V_3$ *collectively* we will solve the band structure of Eq. (4) [replacing $v^{(\alpha)}(|\mathbf{r} - \mathbf{R}_\alpha|)$ by $u_{\text{SLDA}}^{(\alpha)}(|\mathbf{r} - \mathbf{R}_\alpha|)$] and compare the resulting eigenvalues $\tilde{\epsilon}_i$, wave functions $\tilde{\psi}_i$, and related properties with those obtained by solving self-consistently the original LDA Eqs. (1)–(3) for the same structures.

We close this section by noting that if one wishes to perform *non-self-consistent* (e.g., Harris-functional-like¹⁴) electronic structure calculations, $u_{\text{SLDA}}^{(\alpha)}(r)$ can be used as an excellent *input* potential.

B. Using the SLDA to construct the semiempirical pseudopotential method (SEPM)

Our next task is to adjust the SLDA potential of Eq. (14) so that the ensuing wave functions of Eq. (4) will still retain a high overlap with the LDA wave functions of Eqs. (1)–(3), yet the eigenvalues will fit the *experimental* (or quasiparticle calculated) excitations. In this process, the *ab initio* nonlocal potential $\hat{V}_{\text{nonlocal}}(\mathbf{r})$ of Eqs. (2) and (4) (which represents the effects of core electrons) is kept unchanged as in the reference LDA calculations. Furthermore, we use the same analytical form of Eq. (14) for both $u_{\text{SLDA}}^{(\alpha)}(q)$ and $u_{\text{SEPM}}^{(\alpha)}(q)$: the coefficients will change from $C_{\text{SLDA}}^{(\alpha)}(n)$ to $C_{\text{SEPM}}^{(\alpha)}(n)$ while b_n and c_n will be kept fixed.

The fit to the observed excitations is chosen as follows. If P_i denotes the physical property that we wish to reproduce and $M_{n,\alpha}^i = \partial P_i / \partial C_n^{(\alpha)}$ is its derivative with respect to the fitting coefficients $C_n^{(\alpha)}$ of Eq. (14), we will minimize the “cost function”

$$F = \sum_i w_i \left(P_i^{\text{exp}} - P_i^{\text{SLDA}} - \sum_{n,\alpha} M_{n,\alpha}^i \Delta C_n^{(\alpha)} \right)^2 + \sum_{n,\alpha} |\Delta C_n^{(\alpha)}|^2 \omega_{n,\alpha}, \quad (16)$$

where $\Delta C_n^{(\alpha)} \equiv C_{\text{SEPM}}^{(\alpha)}(n) - C_{\text{SLDA}}^{(\alpha)}(n)$ are solutions of the linear equations (16) and w_i and $\omega_{n,\alpha}$ are predetermined weight functions. As will be shown later, the changes from $C_{\text{SLDA}}^{(\alpha)}(n)$ to $C_{\text{SEPM}}^{(\alpha)}(n)$ are rather small; thus the use of a *linear* representation (16) for the fitting process is adequate.¹⁵ A simple choice for the weights

w_i associated with each physical property P_i is to set $w_i = 1/\Delta P_i^2$, where ΔP_i is the acceptable tolerance of P_i (of course, depending on the results of the fit, one can further adjust w_i). The weights $\omega_{n,\alpha}$ can be fixed as $\beta/[|C_{\text{SLDA}}^{(\alpha)}(n)|^2 + |C_{\text{SLDA}}^{(\alpha)}(n+1)|^2]$, where β is an overall scale factor that controls the magnitude of all changes $\Delta C_n^{(\alpha)}$. Fortunately, as will be shown later, only small changes $\Delta C_n^{(\alpha)}$ (i.e., large β) are required to fit the experimental values of P_i . We find that if some P_i cannot be fitted well, this usually reflects internal inconsistency, so increasing $\Delta C_n^{(\alpha)}$ (i.e., reducing β) will not help much. As will be shown later, the closeness of $u_{\text{SEPM}}^{(\alpha)}(q)$ to $u_{\text{SLDA}}^{(\alpha)}(q)$ implies that many properties of the SEPM follow those of the SLDA. These include wave functions, deformation potentials, the transferability between different structures, etc. This closeness provides a control over the quality of the SEPM wave functions, which is lacking in traditional empirical pseudopotential fitting procedures.¹⁶

III. APPLICATIONS TO BULK CdSe AND Si

In this section, we will apply the approach outlined in Sec. II to covalent Si and to partially ionic CdSe, thus covering a range of semiconductor systems.

A. Calculating the spherical and structurally averaged $u_{\text{SLDA}}^{(\alpha)}(q)$

We generate *ab initio* nonlocal pseudopotentials for the LDA calculations of Eq. (2) using the method of Trouillier-Martins.¹² Throughout this paper, we will use the p potential as the local potential, while the s and d are taken as the nonlocal parts. In CdSe, the $4d$ orbitals of Cd are treated as core state and are thus pseudized. This will introduce an error due to the neglect of p - d coupling:¹⁷ for example, the LDA band gap changes from 0.36 eV (with p - d coupling) to 0.74 eV (without p - d coupling). Our *reference* LDA calculation from which the SLDA will be constructed is thus CdSe with pseudized Cd $4d$ orbitals. We solve Eqs. (1) and (4) by expanding ψ in a plane wave basis with cutoff energies E_{cut} . We determine E_{cut} by requiring that the band energies of the pseudopotential calculation match those obtained in an all-electron calculation (with artificially removed p - d coupling). For Si, $E_{\text{cut}} = 20$ Ry is sufficient while for bulk CdSe we need $E_{\text{cut}} = 33$ Ry. To test the convergence of the 33 Ry basis set cutoff and the pseudopotential, we have compared the band energies of CdSe in the wurtzite structure as obtained using the current pseudopotentials and as found using the *all-electron* linear augmented plane wave (LAPW) method in which an artificially deep $4d$ energy is used so that there is no p - d coupling. The average pseudopotential vs LAPW difference in band structure energies is only 84 meV (e.g., aligned by the top of the valence band, the energy differences for Γ_{1c} , Γ_{3v} , M_{4v} , M_{3c} , H_{3v} , and H_{3c} are 120, 55, 11, 119, 10, and 61 meV, respectively). Thus our CdSe

TABLE I. The local, screened LDA pseudopotential $V_{\text{LDA}}(G) = V_{\text{local}} + V_{\text{HXC}}$ [Eq. (5), in eV] and the “strictly forbidden reflection” errors $\Delta V_1(G)$ [Eq. (9), in meV] for CdSe in two crystal structures and different cell volumes per atom Ω . Here, Ω_0 is the equilibrium wurtzite volume per atom and $\mathbf{G} = \frac{2\pi}{a}(h, k, l)$ are reciprocal lattice vectors with Miller indices (h, k, l) . An asterisk means that the structure factor $S(G)$ defined in Eq. (8) is zero for that G .

$ G $ (hkl)	Wurtzite		CdSe		$ G $ (hkl)	Zinc blende		CdSe	
	$\Omega = \Omega_0$		$\Omega = 0.94\Omega_0$			$\Omega = \Omega_0$			
	$V_{\text{LDA}}(G)$ (eV)	$\Delta V_1(G)$ (meV)	$V_{\text{LDA}}(G)$ (eV)	$\Delta V_1(G)$ (meV)		$V_{\text{LDA}}(G)$ (eV)	$\Delta V_1(G)$ (meV)		
(004)	0.5206	56.0	0.4903	54.5	(002)	0.5176	54.8		
(014)	0.1531	8.3	0.1313	7.8	(013)	0.3398	4.1		
(031)	0.0035	3.5*	0.0038	3.8*	(114)	0.2522	1.9		
(033)	0.0019	1.9*	0.0023	2.3*	(024)	0.2090	1.3		
(035)	0.0011	1.1*	0.0014	1.4*	(004)	0.0446	2.8		
(002)	2.186	0	2.188	0	(001)	2.189	0		
(010)	1.529	0	1.533	0	(011)	1.501	0		
(012)	0.510	0	0.511	0	(012)	0.500	0		

pseudopotential with 33 Ry basis set cutoff provides an adequate representation of the all-electron problem, and no core correction¹⁸ is necessary for the purpose of this study.

Using these *ab initio* pseudopotentials and the Ceperley-Alder exchange correlation function,¹⁹ we have performed self-consistent LDA calculations for five CdSe and five Si systems, which are chosen either because they are experimentally achievable or because they have simple structures. The five CdSe systems are (1) the wurtzite structure with atomic volume Ω_0^{CdSe} ; (2) the wurtzite structure with atomic volume $0.944\Omega_0^{\text{CdSe}}$; (3) the zincblende structure with atomic volume Ω_0^{CdSe} ; (4) the rocksalt structure with atomic volume $0.8\Omega_0^{\text{CdSe}}$; and (5) the rocksalt structure with atomic volume Ω_0^{CdSe} . Here, Ω_0^{CdSe} is the experimental equilibrium volume per atom of wurtzite CdSe at ambient pressure (lattice constants $a = 4.30 \text{ \AA}$ and $c/a = \frac{2}{3}\sqrt{6}$). The unit cell volume per atom for each structure is chosen here either from the measured phase transition volume,²⁰ or from LDA calculated equilibrium volumes for that structure. The same is true for Si systems.²¹ Note that both the wurtzite and the zinc blende structures have coordination number of 4, while rocksalt is sixfold coordinated. The five Si systems are (1) the diamond structure with atomic volume Ω_0^{Si} ; (2) the diamond structure with atomic volume $0.92\Omega_0^{\text{Si}}$; (3) the simple cubic structure with atomic vol-

ume $0.82\Omega_0^{\text{Si}}$; (4) the β -tin structure with atomic volume $0.72\Omega_0^{\text{Si}}$ and c/a ratio 0.552; and (5) the simple hexagonal structure with atomic volume $0.69\Omega_0^{\text{Si}}$ and c/a ratio 0.94. Here, Ω_0^{Si} is the measured cell volume per atom of diamondlike Si at ambient pressure (lattice constants $a = 5.43 \text{ \AA}$). The diamond structure of Si is a fourfold coordinated semiconductor, while Si in the simple hexagonal structure is an eightfold coordinated metal.

The self-consistently screened LDA potentials $V_{\text{LDA}}^{(\alpha)}(\mathbf{G}_\sigma)$ are used to solve for $v_{\text{SLDA}}^{(\alpha,\sigma)}$ in Eq. (10). The errors of “strictly forbidden reflections” [Eq. (9)] are listed in Table I for CdSe and in Table II for Si. We note the following: (i) The error ΔV_1 is exactly zero for CdSe in the rocksalt structure and for Si in simple cubic and simple hexagonal structures since there are no “strictly forbidden reflections” because of the high symmetry of these systems. (ii) The “strictly forbidden reflections” error in β -tin (Table II) is small, presumably because its bonding geometry for each atom is close to that of the simple cubic structure and the simple cubic structure has zero “strictly forbidden reflections” error. (iii) The maximum error ΔV_1 has similar values for CdSe in the wurtzite or the zinc blende structures and for Si in diamond structures. All errors are about 60 meV at the primary “forbidden reflections” \mathbf{G}_σ vectors.

Table III reports the “one structure scatter errors” ΔV_2 [Eq. (12)]. Results are given for both CdSe and

TABLE II. Same as Table I (see caption), but for diamondlike and β -tin Si.

$ G $ (hkl)	Diamondlike		Si		$ G $ (hkl)	β -tin		Si	
	$\Omega = \Omega_0$		$\Omega = 0.92\Omega_0$			$\Omega = \Omega_0$			
	$V_{\text{LDA}}(G)$ (eV)	$\Delta V_1(G)$ (meV)	$V_{\text{LDA}}(G)$ (eV)	$\Delta V_1(G)$ (meV)		$V_{\text{LDA}}(G)$ (eV)	$\Delta V_1(G)$ (meV)		
(002)	0.0674	67.4*	0.0656	65.6*	(022)	0.0061	6.1*		
(114)	0.0042	4.2*	0.0048	4.8*	(042)	0.0040	4.0*		
(024)	0.0025	2.5*	0.0027	2.7*	(242)	0.0022	2.2*		
(015)	0.0019	1.9*	0.0019	1.9*	(062)	0.0013	1.3*		
(001)	2.6381	0	2.652	0	(020)	2.4031	0		
(112)	0.5498	0	0.4786	0	(011)	1.4560	0		

TABLE III. The “one structure scatter error” ΔV_2 [Eq. (12)] for particular CdSe structures and cell volumes per atom Ω , and the “structure averaged scatter error” ΔV_3 [Eq. (15)] involving the variance with respect to the structurally averaged potential. Here, Ω_0 is the equilibrium wurtzite CdSe cell volume per atom and Ω'_0 is the equilibrium diamondlike Si cell volume per atom. The numbers in the table are the averaged values of the five largest $\Delta V(|\mathbf{G}|)$'s for that structure. Results for CdSe are given for the “symmetric” [Cd+Se] and antisymmetric [Cd–Se] pieces. The unit is meV.

Structure:	Wurtzite	Wurtzite	Zinc blende	Rocksalt	Rocksalt
Volume Ω :	Ω_0	$0.94\Omega_0$	Ω_0	Ω_0	$0.8\Omega_0$
$\Delta V_2^{(\text{Cd+Se})}/\Omega$	53.9	58.6	1.54	0.36	0.38
$\Delta V_3^{(\text{Cd+Se})}/\Omega$	62.7	72.4	15.2	45.7	19.2
$\Delta V_2^{(\text{Cd–Se})}/\Omega$	9.66	10.3	2.74	0.46	0.82
$\Delta V_3^{(\text{Cd–Se})}/\Omega$	13.5	21.6	11.7	3.48	3.32
Structure:	Diamond	Diamond	β -tin	Simple cubic	Simple hexag.
Volume Ω :	Ω'_0	$0.92\Omega'_0$	$0.72\Omega'_0$	$0.82\Omega'_0$	$0.69\Omega'_0$
$\Delta V_2^{(\text{Si})}/\Omega$	1.69	2.01	6.52	2.82	5.15
$\Delta V_3^{(\text{Si})}/\Omega$	24.0	30.1	15.9	11.3	15.1

Si. We see the following. (i) For wurtzite CdSe, the ΔV_2 error is as large as the “strictly forbidden reflections” error ΔV_1 , while for zinc blende CdSe ΔV_2 is only 5% of ΔV_1 . (ii) For rocksalt CdSe, ΔV_2 is the only source of the spherical approximation error since $\Delta V_1 = 0$. Furthermore ΔV_2 's are very small (~ 0.5 meV). (iii) For all

Si structures, ΔV_2 is of the order of only 5 meV; thus for the diamond structure ΔV_2 is much smaller than the “strictly forbidden reflections” error ΔV_1 . In summary, the spherical approximation errors $\Delta V_1 + \Delta V_2$ for individual structures are of the order of 60 meV for the fourfold coordinated structures and much smaller (~ 1 meV) for the higher coordinated structures.

The solutions $v_{\text{SLDA}}^{(\alpha,\sigma)}(|\mathbf{G}_\sigma|)$ vs $|\mathbf{G}_\sigma|$ of Eq. (10) for CdSe and Si are shown as the diamond symbols in Fig. 1. Instead of showing $v^{(\text{Cd})}$ and $v^{(\text{Se})}$ separately, we have plotted in Fig. 1 the sum $v^{(\text{Cd})} + v^{(\text{Se})}$ and the difference $v^{(\text{Cd})} - v^{(\text{Se})}$. [So the index α in $v_{\text{SLDA}}^{(\alpha,\sigma)}(|\mathbf{G}_\sigma|)$ is not Cd and Se, but the symmetric Cd+Se part and the antisymmetric Cd–Se part.] The zero momentum $v_{\text{SLDA}}^{(\text{Cd},\sigma)}(0) + v_{\text{SLDA}}^{(\text{Se},\sigma)}(0)$ and $v_{\text{SLDA}}^{(\text{Si},\sigma)}(0)$ points are arbitrary in bulk LDA calculations. They were calculated here from the work functions of wurtzite CdSe (Refs. 22 and 23) and diamondlike Si (Ref. 24) crystals. The difference $v_{\text{SLDA}}^{(\text{Cd},\sigma)}(0) - v_{\text{SLDA}}^{(\text{Se},\sigma)}(0)$ represents the average potential difference between pure bulk Cd and pure bulk Se. This difference was taken here as the potential difference between the Cd bulk region and the Se bulk region in a supercell calculation which consists of a few monolayers of Cd and a few monolayer of Se on a simple cubic lattice. *The important result demonstrated in Fig. 1 is that $v_{\text{SLDA}}^{(\alpha,\sigma)}(|\mathbf{G}_\sigma|)$ of different structures and unit cell volumes all fall on a nearly universal curve for a given α .*

The structurally averaged and least square fitted curves $u_{\text{SLDA}}^{(\alpha)}(q)$ of Eq. (14) are shown in Figs. 1(a)–1(c) as solid lines. The fit is excellent. The “structure averaged scatter errors” ΔV_3 calculated using $u_{\text{SLDA}}^{(\alpha)}(q)$ in Eq. (15) are reported in Table III for CdSe and Si. Now the errors are typically of the order of 20–70 meV for all structures. We can thus conclude that structural averaging is the largest source of error in $u_{\text{SLDA}}^{(\alpha)}(q)$ for the higher coordinated structures. On the other hand, for the lower (fourfold) coordinated structures, the structural averaging error ΔV_3 has similar magnitude as the spherical approximation errors $\Delta V_1 + \Delta V_2$ for individual structures. The *overall* error in $u_{\text{SLDA}}^{(\alpha)}(q)$ for all struc-

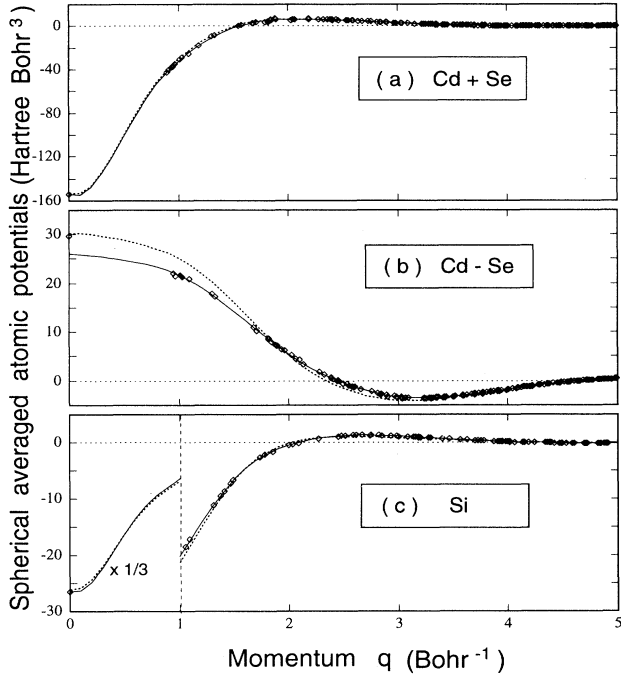


FIG. 1. The spherical LDA (SLDA) potential $v_{\text{SLDA}}^{(\alpha,\sigma)}(|\mathbf{G}_\sigma|)$ [Eq. (10)] as obtained from self-consistent bulk LDA calculations on five crystal structures and cell volumes. Diamond symbols show the numerical results obtained by solving Eq. (10) for all five structures. Solid lines represent least square fits of all the diamond symbols using the analytic expression of Eq. (14). Dashed lines represent the empirically adjusted potential (SEPM) fit to the experimental excitations. For CdSe, we give the symmetric $v^{\text{Cd}} + v^{\text{Se}}$ potential as well as the antisymmetric $v^{\text{Cd}} - v^{\text{Se}}$ part.

tures is as small as ≤ 70 meV. This suggests a good structural transferability of $u_{\text{SLDA}}^{(\alpha)}(q)$.

To examine this point we compare the band structures obtained using in Eq. (4) $u_{\text{SLDA}}^{(\alpha)}(q)$ with the band structure obtained in direct LDA calculations. This comparison is given in Tables IV for CdSe in the wurtzite structure, in Table V for CdSe in the rocksalt structure, and in Table VI for CdSe in the zinc blende structure and a deformed wurtzite structure. The root mean square (rms) differences between LDA and SLDA band energies are about 50 meV, consistent with the overall error in $u_{\text{SLDA}}^{(\text{Cd,Se})}(q)$ discussed above. To see the effects of hydrostatic pressure we give in Tables IV and V the energy difference $\epsilon(\Omega_0) - \epsilon(\Omega_1)$ for two unit cell volumes (Ω_0 and Ω_1) as computed in the LDA and SLDA methods. This comparison shows that the average error in hydrostatic deformation potential of SLDA relative to that of LDA is about 20% for wurtzite CdSe and 8% for rocksalt CdSe. Besides the five CdSe structures mentioned above, we give in Table VI the band energies of wurtzite CdSe but with randomly displaced atoms (of the order of 4% of the bond length). The band energy difference $\epsilon_i\{R_i + \delta\} - \epsilon_i\{R_i\}$ between this deformed structure $\{R_i + \delta\}$ and the original wurtzite structure $\delta = 0$ reflects phonon deformation potentials. The average phonon deformation potential difference between the LDA and SLDA is about 20%.

For Si systems, instead of showing all the band edge states as we did for CdSe, we give in Table VII only the rms and maximum band energy differences between the SLDA and LDA. Here, we include most high symmetry points for each structure (e.g., L , Γ , X , and K for the diamond structure) and all eigenstates up to ~ 4 eV above the conduction band minimum for semiconductors and ~ 4 eV above the Fermi energy for metals. The average

SLDA vs LDA energy difference is about 60 meV, similar to the potential error of $u_{\text{SLDA}}^{(\text{Si})}(q)$. Notably, the energy errors for simple cubic, simple hexagonal, and β -tin structures are much smaller (~ 15 meV) than those for the diamond structure. This is consistent with the fact that the potential errors (Table III) of the former structures are smaller than those in the diamond structure. The hydrostatic deformation potential difference between the SLDA and LDA is about 18% for the diamond structure. Table VII gives the energies of the diamond structure with randomly displaced Si atoms (by 10% of the bond length). The error in the phonon deformation potential is about 14%. Table VII also shows predictions for additional crystal structures, *not used in our fits*. These include the fourfold coordinated $BC8$ structure,²⁵ which has eight Si atoms per unit cell and an atomic volume of $0.91\Omega_0^{\text{Si}}$. The average SLDA vs LDA band energy error is 75 meV, only slightly larger than the errors for the structures included in the fit. We also tested the simple face centered cubic structure, which is a 12-fold coordinated system with an atomic volume of $0.72\Omega_0^{\text{Si}}$. The average SLDA vs LDA energy error is also 75 meV.

To summarize the energy errors we can say that the spherical and structurally averaged potential $u_{\text{SLDA}}^{(\alpha)}(q)$ reproduces the original self-consistent LDA band energies to within ~ 0.1 eV or better for a range of different crystal structures, including those not used in its construction.

We next discuss the accuracy of $u_{\text{SLDA}}^{(\alpha)}(q)$ in reproducing LDA *wave functions* and related properties. To this end, we have calculated the overlap between the SLDA wave functions ψ_i [Eq. (4)] and the LDA wave functions ψ_i [Eqs. (1)–(3)]. The results for CdSe in the wurtzite structure and for Si in the diamond structure are listed in Table VIII, where wave functions up to about 4 eV above

TABLE IV. Comparison of band energies ϵ_i (in eV) of high symmetry band edge states of CdSe in the wurtzite structure as obtained by the original LDA, the LDA with spherically averaged local potentials (SLDA), and the empirically adjusted LDA (SEPM). rms denotes the root mean square difference between LDA and SLDA results. We show band energies at the equilibrium cell volume Ω_0 as well as the difference in band energies at two cell volumes (proportional to the hydrostatic deformation potential). Both the LDA and the SLDA use basis set cutoff of $E_{\text{cut}} = 33$ Ry, while the SEPM is calculated with a reduced cutoff of 6.8 Ry plus a compensating Gaussian (G) correction discussed in Sec. III B. The zero of energy is at the top of the valence band.

E_{cut} (Ry):	Wurtzite CdSe $\epsilon_i(\Omega = \Omega_0)$			$\epsilon_i(\Omega = 0.94\Omega_0) - \epsilon_i(\Omega = \Omega_0)$		
	LDA	SLDA	SEPM	LDA	SLDA	SEPM
Γ_{1c}	0.858	0.870	1.847	0.218	0.250	0.252
$A_{5,6v}$	-0.366	-0.371	-0.331	-0.041	-0.039	-0.044
$A_{1,3c}$	2.590	2.592	3.434	0.176	0.209	0.203
$L_{1,3v}$	-1.195	-1.194	-1.165	-0.130	-0.120	-0.151
$L_{1,3c}$	3.102	3.122	3.792	0.074	0.119	0.134
M_{4v}	-0.659	-0.662	-0.702	-0.074	-0.070	-0.079
M_{3c}	3.451	3.498	4.218	0.028	0.081	0.077
H_{3v}	-0.978	-0.987	-0.976	-0.102	-0.097	-0.134
H_{3c}	3.912	3.957	4.693	0.139	0.173	0.209
K_{3v}	-1.570	-1.557	-1.588	-0.169	-0.150	-0.154
K_{2c}	4.438	4.467	4.742	-0.085	-0.011	0.025
rms diff.		0.023			0.036	

TABLE V. Same as Table IV (see caption), but for rocksalt CdSe.

E_{cut} (Ry):	Rocksalt CdSe $\epsilon_i(\Omega = 0.8\Omega_0)$			$\epsilon_i(\Omega = 0.8\Omega_0) - \epsilon_i(\Omega = \Omega_0)$		
	LDA	SLDA	SEPM	LDA	SLDA	SEPM
	33	33	6.8+G	33	33	6.8+G
Γ_{1c}	0.766	0.808	1.727	1.176	1.263	1.172
L_{3v}	0.282	0.267	0.316	0.153	0.143	0.196
L_{1c}	3.548	3.451	4.009	0.269	0.367	0.414
X_{5v}	-1.636	-1.664	-1.568	-0.481	-0.464	-0.402
X_{1c}	-0.235	-0.208	1.055	0.294	0.358	0.421
K_{4v}	-1.059	-1.086	-0.985	-0.309	-0.299	-0.228
K_{1c}	1.835	1.833	2.809	0.477	0.516	0.598
Σ_{4v}	0.381	0.374	0.385	0.155	0.146	0.177
Σ_{1c}	3.854	3.874	4.491	1.297	1.327	1.315
rms diff.		0.040			0.052	

the conduction band minimum are included. For both systems, the average overlap $\langle \psi_i | \psi_i \rangle$ is above 99.99%, while the minimum overlap is about 99.97%. This agreement is excellent.

A more stringent test of wave function quality is to compare the momentum matrix elements $M_{if} = \langle \psi_i | \hat{p} | \psi_f \rangle$, since a small change in the wave function can lead to a large change in this quantity. Table IX compares the momentum matrix elements squared as computed with LDA and SLDA wave functions. We see that they follow each other very closely, with typical errors less than 1%.

TABLE VI. Same as Table IV (see caption), but for the zinc blende and a deformed wurtzite structure of CdSe. We show band energies at the equilibrium cell volume Ω_0 for zinc blende as well as the difference in band energies between the deformed and the original wurtzite structures (proportional to the phonon deformation potential).

E_{cut} (Ry):	LDA	SLDA	SEPM
	Zinc blende	CdSe	$\epsilon_i(\Omega_0)$
	33	33	6.8+G
Γ_{1c}	0.837	0.829	1.733
L_{3v}	-0.644	-0.652	-0.603
L_{1c}	2.593	2.550	3.612
X_{5v}	-1.604	-1.625	-1.553
X_{1c}	3.347	3.258	3.875
K_{2v}	-1.320	-1.338	-1.265
K_{3c}	3.907	3.833	4.599
rms		0.048	
	Deformed wurtzite	CdSe	$\epsilon_i\{R_i + \delta\} - \epsilon_i\{R_i\}$
Γ_{6v}	0.096	0.156	0.162
Γ_{1c}	0.016	0.017	-0.007
$A_{5,6v}$	0.177	0.143	0.165
$A_{1,3c}$	-0.243	-0.191	-0.124
$L_{1,3v}$	0.208	0.277	0.342
$L_{1,3c}$	0.019	0.017	0.015
M_{4v}	-0.123	-0.144	-0.083
M_{3c}	-0.189	-0.154	-0.126
H_{3v}	0.270	0.319	0.350
H_{3c}	-0.125	-0.088	-0.156
K_{3v}	0.113	0.181	0.289
K_{2c}	0.239	0.237	0.228
rms diff.		0.043	

Given the momentum matrix elements M_{if} , the absorption spectra can be calculated as

$$\epsilon_2(E) = \frac{8\pi^2}{3\Omega} \sum_{i,f} \frac{M_{if}^2}{(E_f - E_i)} \delta(E - E_f + E_i), \quad (17)$$

while the static dielectric constant is given by

$$\epsilon_s = 1 + \frac{2}{\pi} \int_0^\infty \frac{\epsilon_2(E)}{E} dE, \quad (18)$$

where i and f denote the initial and final states. From perturbation theory,²⁶ we know that to get the correct response function [thus $\epsilon_2(E)$ and ϵ_s] under Hamiltonian \hat{H} , we should replace M_{if} by $\langle \psi_i | \frac{\partial \hat{H}}{\partial k} | \psi_f \rangle$. In our case of a *nonlocal* pseudopotential Hamiltonian, one needs to use $\partial \hat{H} / \partial k = \hat{p} + \partial \hat{V}_{\text{nonlocal}} / \partial k$. For the sake of comparison and to understand how much each term contributes, we have calculated, however, $\epsilon_2(E)$ and ϵ_s by using both the momentum \hat{p} and the $\hat{p} + \partial \hat{V}_{\text{nonlocal}} / \partial k$ as the matrix element M_{if} . The results for ϵ_s are listed in Table X. The differences between the LDA and SLDA are only about 2%.

In summary, the wave functions, transition matrix elements, and dielectric constants obtained with the spherical and structural averaged atomic potential $u_{\text{SLDA}}^{(\alpha)}(q)$ reproduce the original self-consistent LDA calculations extremely well.

B. Reducing the size of the plane wave basis set

We are now at the point of modifying $u_{\text{SLDA}}^{(\alpha)}(q)$ to obtain the SEPM potentials. However, before doing so, we would like to reduce the number of plane wave basis functions needed to solve the Schrödinger equations with the SLDA. The motivation here is purely practical: After all, the purpose of developing an empirical pseudopotential is to perform fast computations for large systems. The converged cutoff energies of 20 Ry for Si and 33 Ry for CdSe correspond to about 250 and 500 plane waves per atom; this is excessive for large system calculations.⁴⁻⁷ We would like to reduce the cutoff energy to about 5 Ry,

TABLE VII. Band structure error $\epsilon_i^{\text{SLDA}} - \epsilon_i^{\text{LDA}}$ (in meV) for Si systems. The root mean square (rms) errors and the maximum errors of the high symmetry band energies for each structure are listed. We include in the statistics most high symmetry states (e.g., L , Γ , X and K for the diamond structure) and average over band energies up to ~ 4 eV above the conduction band minimum or Fermi level. $E_{\text{cut}} = 20$ Ry is used for all the calculations. The values in the parentheses of $\epsilon_i()$ denote the cell volume per atom and Ω_0 is the equilibrium cell volume per atom of diamondlike Si. The SLDA vs LDA error in the hydrostatic deformation potential in column 4 is about 18% and the relative error of the phonon deformation potentials in column 5 is about 14%. The $BC8$ and fcc structures were not included in the fit of the SLDA potential.

Si structure:	Diamond	Diamond	Diamond	Deformed diamond	Simple cubic
SLDA-LDA:	$\epsilon_i(\Omega_0)$	$\epsilon_i(0.92\Omega_0)$	$\epsilon_i(\Omega_0) - \epsilon_i(0.92\Omega_0)$	$\epsilon_i\{R + \delta\} - \epsilon_i\{R\}$	$\epsilon_i(0.82\Omega_0)$
rms error:	46	69	59	66	10
Max error:	97	136	201	176	22
Si structure:	sh	β -tin	BC8	fcc	
SLDA-LDA:	$\epsilon_i(0.69\Omega_0)$	$\epsilon_i(0.72\Omega_0)$	$\epsilon_i(0.91\Omega_0)$	$\epsilon_i(0.72\Omega_0)$	
rms error:	16	15	75	75	
Max error:	43	41	270	122	

so there are only about 30 plane waves per atom.

With a small energy cutoff, the band energies are usually not converged with regard to the basis. As a result, there will be a discontinuity in the band energies vs Bloch function wave vector k , since the number of plane wave basis functions changes discontinuously as a function of k . (This error can appear in large supercell calculations even though only the Γ point energy is used, due to the folding of off- Γ states.) To correct for this error, we have used a smooth cutoff which smears out the discontinuity. This smooth cutoff is only used for CdSe systems. For Si systems, the conventional abrupt cutoff is used. The details are given in Appendix A. We also developed a way of implementing the nonlocal potential in a plane wave basis calculation so that the $\hat{H}\psi$ operation scales *linearly* with the size of the system. This is called “small box implementation of the nonlocal potential” and is fast when E_{cut} is small. The details of this method are given

in Appendix B.^{27–30}

While the “small box” implementation involves only small numerical errors, the use of a small basis set can have a dramatic effect on the band energies. Shown in Fig. 2(a) and Fig. 3(a) are the SLDA band structures of wurtzite CdSe and diamondlike Si, using a high E_{cut} (33 Ry for CdSe, 20 Ry for Si) and a low E_{cut} (6.8 Ry for CdSe and 5.6 Ry for Si). [The high E_{cut} LDA results (not shown) are almost indistinguishable from the high E_{cut} SLDA curves in Fig. 2(a) and Fig. 3(a).] Significant differences in band energies are apparent, with the largest difference occurring at the s -like states. Based on this observation, a simple solution is found: we add to the s nonlocal potential a negative Gaussian term $-V_G^{(\alpha)} e^{-[r/R_G^{(\alpha)}]^2}$ pulling down the s state energy. By adjusting $V_G^{(\alpha)}$ and $R_G^{(\alpha)}$, we have arrived at the following solutions: for Se in CdSe systems, $V_G^{(\text{Se})} = 3.72$ Ry

TABLE VIII. Wave function overlaps $|\langle\psi_i|\psi'_i\rangle|$ where ψ_i and ψ'_i are obtained by using different potentials in the Schrödinger equation. Here, LDA, SLDA, and SEPM denote, respectively, the LDA [Eqs. (1)–(3)], the LDA with spherically symmetrized local potential and the empirically adjusted SLDA. For CdSe in the wurtzite structure we considered wave functions at the Γ point and bands up to 4 eV above the conduction band minimum, while for diamondlike Si wave functions at the Γ , X , and K points and bands up to 4 eV above the conduction band minimum are considered. The numbers in the parentheses denote the plane wave basis energy cutoff E_{cut} (in Ry), while “6.8+ G ” and “5.6+ G ” are defined as in Table IV (see caption). The root mean square (rms) and the minimum overlap of the wave functions are listed. BC stands for the Bergstresser and Cohen empirical pseudopotential for CdSe (Ref. 34), while CC denote the Chelikowsky and Cohen nonlocal Si empirical pseudopotential (Ref. 35).

$ \langle\psi_i \psi'_i\rangle $ for wurtzite CdSe					
ψ_i	LDA(33)	SLDA(33)	LDA(33)	SLDA(6.8+ G)	LDA(33)
ψ'_i	SLDA(33)	SLDA(6.8+ G)	SEPM(33)	SEPM(6.8+ G)	BC(33)
rms	0.99991	0.986	0.998	0.998	0.970
min	0.99982	0.971	0.995	0.996	0.923
$ \langle\psi_i \psi'_i\rangle $ for diamondlike Si					
ψ_i	LDA(20)	SLDA(20)	LDA(20)	SLDA(5.6+ G)	LDA(20)
ψ'_i	SLDA(20)	SLDA(5.6+ G)	SEPM(20)	SEPM(5.6+ G)	CC(20)
rms	0.99998	0.987	0.9998	0.9998	0.994
min	0.99971	0.983	0.9993	0.9994	0.987

TABLE IX. Momentum matrix elements $M_{if}^2 = |\langle \psi_i | \hat{p} | \psi_f \rangle|^2$ for wurtzite CdSe and for diamondlike Si as obtained by various approximations. Here, LDA, SLDA, and SEPM denote, respectively, the LDA [Eqs. (1)–(3)], the LDA with spherically symmetrized local potential, and the empirically adjusted SLDA. The unit for M_{if}^2 is bohr⁻². The notations “6.8+G” and “5.6+G” are defined as in Table IV (see caption). EPM stands for the Bergstresser-Cohen empirical pseudopotential for CdSe (Ref. 34) and for the Chelikowsky-Cohen nonlocal empirical pseudopotential for Si (Ref. 35). \perp and \parallel denote perpendicular and parallel to the c axis of the wurtzite structure, respectively.

	LDA	SLDA	SLDA	SEPM	EPM
E_{cut} for CdSe (Ry)	33	33	6.8+G	6.8+G	33
E_{cut} for Si (Ry)	20	20	5.6+G	5.6+G	20
$ \langle i \hat{p}_{\perp} f \rangle ^2$ for wurtzite CdSe					
$\Gamma'_{1v} - \Gamma_{6v}$	0.145	0.144	0.141	0.152	0.295
$\Gamma'_{3v} - \Gamma_{5v}$	0.170	0.169	0.168	0.179	0.301
$\Gamma_{5v} - \Gamma_{3c}$	0.311	0.313	0.324	0.320	0.306
$\Gamma_{5v} - \Gamma_{6c}$	0.380	0.382	0.360	0.386	0.490
$ \langle i \hat{p}_{\parallel} f \rangle ^2$ for wurtzite CdSe					
$\Gamma'_{1v} - \Gamma_{1v}$	0.107	0.106	0.106	0.116	0.222
$\Gamma'_{3v} - \Gamma_{3v}$	0.190	0.189	0.196	0.201	0.234
$\Gamma_{1v} - \Gamma_{1c}$	0.208	0.208	0.227	0.218	0.159
$\Gamma_{1v} - \Gamma'_{1c}$	0.241	0.242	0.231	0.237	0.315
$ \langle i \hat{p}_z f \rangle ^2$ for diamondlike Si					
$\Gamma_{1c} - \Gamma_{15c}$	0.025	0.025	0.026	0.029	0.038
$\Gamma_{25'v} - \Gamma_{15c}$	0.546	0.550	0.532	0.533	0.533
$X_{1v} - X_{1c}$	0.122	0.122	0.115	0.122	0.123
$K_{1v} - K_{3v}$	0.140	0.140	0.147	0.144	0.151
$K_{3v} - K'_{1v}$	0.123	0.124	0.126	0.120	0.128
$K_{5c} - K_{1c}$	0.0094	0.0093	0.0082	0.0097	0.0072

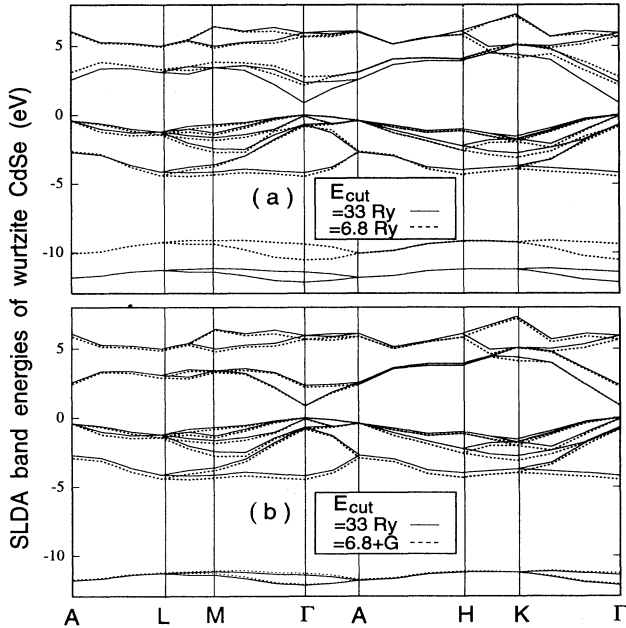


FIG. 2. SLDA band structure of CdSe in the wurtzite structure as obtained with different basis set cutoff energies (E_{cut}). Solid lines in (a) and (b): large cutoff of 33 Ry; dashed line in (a): small cutoff of 6.8 Ry; dashed line in (b): small cutoff with a compensating Gaussian (G) correction. The zero of the energy is at the top of the valence band.

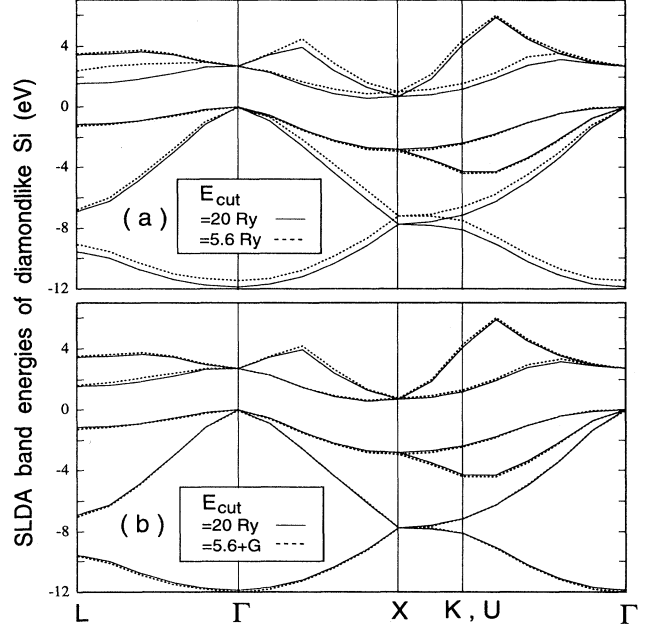


FIG. 3. SLDA band structure of Si in the diamond structure as obtained with different basis set cutoff energies (E_{cut}). Solid lines in (a) and (b): large cutoff of 20 Ry; dashed line in (a): small cutoff of 5.6 Ry; dashed line in (b): small cutoff with a compensating Gaussian (G) correction. The zero of the energy is at the top of the valence band.

and $R_G^{(\text{Se})} = 0.37 \text{ \AA}$ while no correction is needed for Cd. In Si systems, $V_G^{(\text{Si})} = -6 \text{ Ry}$ and $R_G^{(\text{Si})} = 0.265 \text{ \AA}$.

In Fig. 2(b) and Fig. 3(b), the Gaussian corrected SLDA band structures with low E_{cut} are compared with the high E_{cut} SLDA results. Comparing to Figs. 2(a) and 3(a), it is clear that the band energy error has been mostly corrected. The same is true for other crystal structures. Especially interesting is the behavior of the hydrostatic deformation potential and the phonon deformation potentials: We find that the Gaussian corrected low E_{cut} SLDA has similar deformation potential errors as the high E_{cut} SLDA when compared to the high E_{cut} LDA results. The change of ϵ_s from high E_{cut} calculation to low E_{cut} but Gaussian corrected calculation is about 7% as shown in Table X. More detail discussions are given in Ref. 31.

In summary, when E_{cut} is lowered to about 5 Ry, there are large band structure errors. However, when a Gaussian potential is added to the s nonlocal potential, most properties are restored to their high E_{cut} values. The physical properties we tested include band energies, wave functions, transition matrix elements, density of states, and dielectric constants. Although this step of lowering E_{cut} might be numerically the most severe approximation in our whole procedure, we find satisfactory results in all tested properties.

C. Fitting the SLDA potential to the SEPM

We next will fit $u_{\text{SLDA}}^{(\alpha)}(q)$ to get the semiempirical potential $u_{\text{SEPM}}^{(\alpha)}(q)$ using Eqs. (14) and (16). The low E_{cut} and the Gaussian corrections are kept fixed as is the nonlocal part of the LDA pseudopotential $\hat{V}_{\text{nonlocal}}$. The fitting procedure follows the outline in Sec. II. Equation (16) has been iterated 2–3 times, as described in Ref. 15. For CdSe, we now also include in the Hamiltonian the spin-orbit interaction. This is done by adding to the Hamiltonian the relativistic LDA (nonlocal) spin-orbit pseudopotential term, and, at the same time, expanding the wave function ψ in terms of spin up ψ_{\uparrow} and spin down ψ_{\downarrow} components (see Appendix B and Ref. 30). The nonlocal spin-orbit term was generated by the atomic pseudopotential generator,¹² and is used without any modifications. Only ten of the coefficients $C^{(\alpha)}(n)$ of Eq. (14) for each α out of a total of 20 $C^{(\alpha)}(n)$'s have been modified in Eq. (16). This corresponds to the modification of $u_{\text{SLDA}}^{(\alpha)}(q)$ in the region of $0 \leq q \leq 5 \text{ bohr}^{-1}$.³²

The resulting $u_{\text{SEPM}}^{(\alpha)}(q)$ is shown as dashed lines in Figs. 1(a) and 1(b) for CdSe and Fig. 1(c) for Si. The change from $u_{\text{SLDA}}^{(\alpha)}(q)$ to $u_{\text{SEPM}}^{(\alpha)}(q)$ [Figs. 1(a)–(c)] is very small. Figures 4 and 5 show the difference $u_{\text{SEPM}}^{(\alpha)} - u_{\text{SLDA}}^{(\alpha)}$ in momentum and real space, respectively. While this difference depends on the details of the fit, we can see that the changes are rather small and located around the bond center region in the solid.

The local and nonlocal SLDA and SEPM potentials for Si and for CdSe are deposited in an anonymous FTP site³³ in a numerical form, so interested readers can get them electronically.

D. SEPM results and comparison with the traditional EPM

In this section, we will show our SEPM results and compare them with the results of the traditional

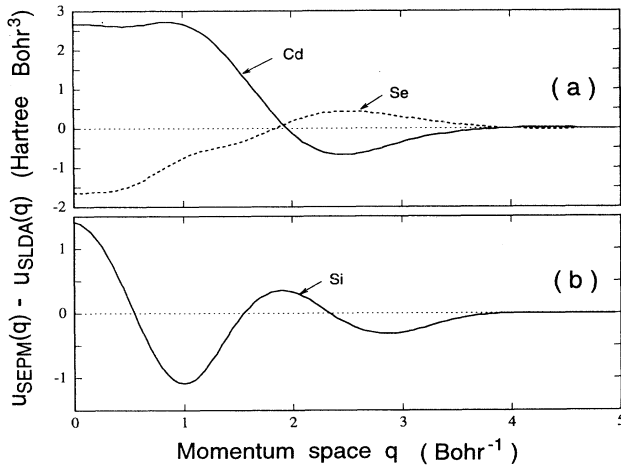


FIG. 4. Potential difference $u_{\text{SEPM}}^{(\alpha)} - u_{\text{SLDA}}^{(\alpha)}$ in momentum space for (a) Cd and Se and (b) Si. These are the p state potentials and are used as the local potentials in the calculation.

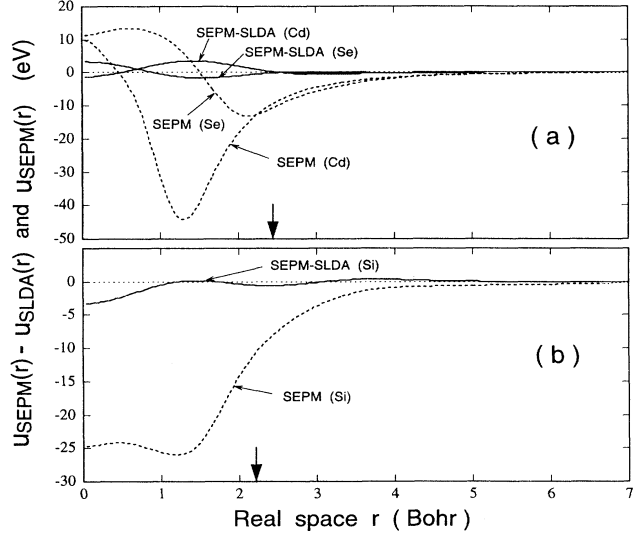


FIG. 5. Potential differences $u_{\text{SEPM}}^{(\alpha)} - u_{\text{SLDA}}^{(\alpha)}$ and the semiempirical pseudopotentials $u_{\text{SEPM}}^{(\alpha)}$ in real space for (a) Cd and Se and (b) Si. These are the p state potentials and are used as the local potentials in the calculation. The vertical arrows indicate the bond center locations in the equilibrium (a) wurtzite and (b) diamond structures.

Bergstresser and Cohen³⁴ (BC) local empirical pseudopotential for CdSe and with the Chelikowsky and Cohen³⁵ (CC) nonlocal empirical pseudopotential for Si. The comparison is done for (a) the band structure, (b) the wave functions, and (c) the optical properties.

(a) *SEPM band energies.* The fitted experimental quantities P_i (Refs. 36–55) and their SEPM results are listed in Table XI for CdSe and in Table XII for Si. To see the modification from SLDA to SEPM, we also listed the physical quantities calculated from the SLDA. For Si, our SEPM band structure has a similar quality as the (already accurate) Chelikowsky-Cohen nonlocal empirical pseudopotential. The results of *GW* quasiparticle calculations³⁶ are also listed in Table XI for CdSe to compare with our results and experiments. For CdSe, our SEPM result has a much better quality, especially for the upper valence bandwidth, compared to the Bergstresser-Cohen local empirical pseudopotential. For CdSe in the rocksalt structure, our SEPM conduction band minimum is at X point and valence band maximum is on the Σ line. These are consistent with the experimental results⁵⁶ and *GW* quasiparticle calculations.³⁶ To see the trend, we have listed the SEPM band energies in Tables IV, V, and VI for CdSe structures. Note that both the hydrostatic and phonon deformation potential of the SEPM follow closely those of LDA and SLDA results. This is one of the advantages of using the SLDA as our starting potential in the fitting procedure. The SEPM inherits many of the correct properties of the SLDA (hence LDA) without explicit fitting. Finally, the band structures of wurtzite and rocksalt CdSe using the SEPM with spin-orbit coupling are shown in Fig. 6 (Ref. 57) and Fig. 7, respectively, and the band structure of diamondlike Si

TABLE X. The static dielectric constants ϵ_s of CdSe and Si as calculated using Eqs. (17) and (18) and different sources for the transition matrix element M_{if} between initial (i) and final (f) electronic states. \hat{p} denotes the momentum operator, while \hat{V} , \hat{G} , and \hat{W} are the nonlocal potential, the s nonlocal Gaussian correction, and the smooth E_{cut} operation, respectively, as discussed in Ref. 31. k denotes a wave vector in the bulk Brillouin zone. LDA, SLDA, and SEPM denote, respectively, the LDA [Eqs. (1)–(3)], the LDA with spherically symmetrized local potential, and the empirically adjusted SLDA. EPM stands for the Bergstresser-Cohen empirical pseudopotential for CdSe (Ref. 34) and the Chelikowsky-Cohen nonlocal empirical pseudopotential for Si (Ref. 35). The correct matrix element form is $M_{if} = \langle i | \partial \hat{H} / \partial k | f \rangle$ when compared to the experiment. \perp and \parallel denote perpendicular and parallel to the c axis of the wurtzite structure, respectively.

	LDA	SLDA	SLDA	SEPM	EPM
E_{cut} for CdSe (Ry)	33	33	6.8+ G	6.8+ G	33
E_{cut} for Si (Ry)	20	20	5.6+ G	5.6+ G	20
	CdSe wurtzite		$\epsilon_s(\perp)$		
$M_{if} = \langle i \hat{p} f \rangle$	6.40	6.34	6.52	4.66	4.85
$M_{if} = \langle i \hat{p} + \frac{\partial \hat{V}}{\partial k} f \rangle$	7.16	7.07	7.30	5.19	
$M_{if} = \langle i \hat{p} + \frac{\partial}{\partial k} (\hat{V} + \hat{G}) f \rangle$			7.48	5.31	
$M_{if} = \langle i \hat{p} + \frac{\partial}{\partial k} (\hat{V} + \hat{G} + \hat{W}) f \rangle$			7.63	5.40	
	CdSe wurtzite		$\epsilon_s(\parallel)$		
$M_{if} = \langle i \hat{p} f \rangle$	6.43	6.32	6.64	4.88	4.68
$M_{if} = \langle i \hat{p} + \frac{\partial \hat{V}}{\partial k} f \rangle$	7.15	7.01	7.33	5.37	
$M_{if} = \langle i \hat{p} + \frac{\partial}{\partial k} (\hat{V} + \hat{G}) f \rangle$			7.50	5.49	
$M_{if} = \langle i \hat{p} + \frac{\partial}{\partial k} (\hat{V} + \hat{G} + \hat{W}) f \rangle$			7.61	5.57	
	Si diamond		ϵ_s		
$M_{if} = \langle i \hat{p} f \rangle$	16.49	16.11	14.38	12.26	10.58
$M_{if} = \langle i \hat{p} + \frac{\partial \hat{V}}{\partial k} f \rangle$	14.09	13.78	12.82	10.91	10.33
$M_{if} = \langle i \hat{p} + \frac{\partial}{\partial k} (\hat{V} + \hat{G}) f \rangle$			12.88	10.95	

using the SEPM is shown in Fig. 8.

(b) *SEPM wave functions.* In Table VIII we show the wave function overlap between the SEPM and LDA. In the same table, we also list the wave function overlaps using the traditional empirical pseudopotentials of Bergstresser-Cohen and Chelikowsky-Cohen. To com-

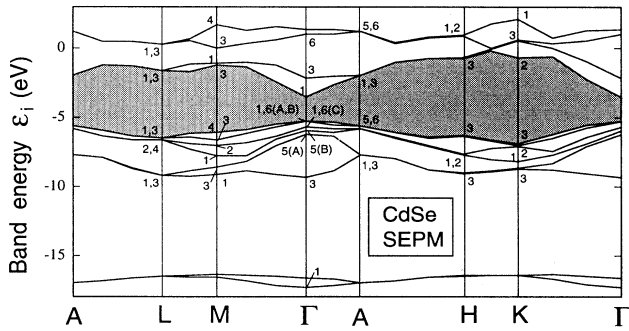


FIG. 6. SEPM band structure of CdSe in the wurtzite structure with spin-orbit interaction. Only spin up band energies are shown (The spin down band energies can be 0.1 eV different from the spin up band energies at low symmetry points.) The plane wave cutoff energy is 6.8 Ry; a Gaussian compensating s potential is used. The zero of the energy is the vacuum level. To simplify the comparison with experiment, the “single” space group representation (instead of “double” space group representation, Ref. 57) is used for the band state notation. The spin-orbit splitting is indicated by A, B, and C in the parentheses.

pare the different overlaps properly, we compare $\langle \psi_i | \psi_i' \rangle$ with the same E_{cut} basis for both ψ_i and ψ_i' . For CdSe, the overlap of the Bergstresser-Cohen wave function with the LDA wave function is on average only 97%, the minimum overlap being 92%. On the other hand, the overlap of the SEPM wave function with the LDA (and SLDA) wave function is 99.8% on average, the minimum being 99.5%. For Si, the Chelikowsky-Cohen nonlocal EPM wave function overlap with the LDA result is 99.4% on average, the minimum being 98.7%. On the other hand, the overlap of the SEPM wave function with the LDA (and SLDA) wave function is 99.98% on average, the minimum being 99.94%. Thus SEPM wave functions are 10 times closer to their LDA counterparts than the tradi-

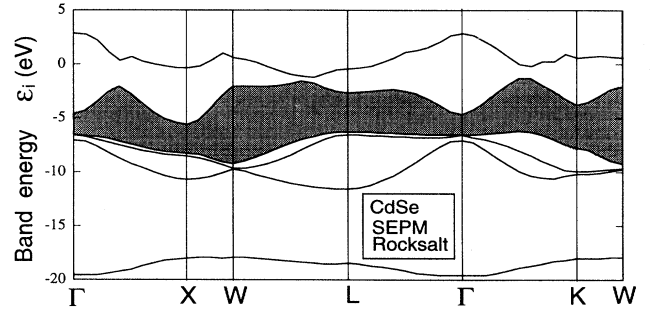


FIG. 7. SEPM band structure of CdSe in the rocksalt structure with spin-orbit interaction. Only spin up band energies are shown. The plane wave cutoff energy is 6.8 Ry; a Gaussian compensating s potential is used. The zero of the energy is the vacuum level.

tional EPM wave functions.

In Table IX, we have listed the matrix elements $|\langle\psi_i|\hat{p}|\psi_f\rangle|^2$ of the SEPM results and the traditional EPM results for CdSe wurtzite structure and Si diamond structure. The matrix elements of the SEPM follow closely the LDA and SLDA results. On the other hand, the matrix elements of the traditional EPM may sometimes differ from LDA results by a factor of 2.

(c) *SEPM optical properties.* The SEPM density of states and the dielectric constants $\epsilon_2(E)$ are shown in Figs. 9(a)–9(c) for CdSe and Figs. 10(a) and 10(b)

for Si. The density of states compares very well with the experimental data,^{58,59} especially the peak positions. For CdSe, however, there are a number of discrepancies caused by the neglect of the Cd 4*d* orbits in our pseudopotential treatment. (i) The width of the CdSe upper valence band in Fig. 9(a) is smaller than the experimental value. This is partly caused by our neglect of the Cd 4*d* states. Because of *p-d* coupling, the 4*d* state will push up the top of the valence band resulting in an increased upper valence band width. (ii) The optical absorption spectrum $\epsilon_2(E)$ of CdSe agrees very well with the exper-

TABLE XI. Comparison for CdSe of band energies (in eV), band gap E_g (in eV), and effective masses (in units of electron mass) as obtained in the LDA, the LDA with spherically symmetric local potential (SLDA), the semiempirical SEPM, the traditional empirical pseudopotential method (EPM) (Ref. 34), *GW* quasiparticle calculations (Ref. 36), and experiments. See Fig. 6 for the identity of the various band state notations used in this table. The LDA, SLDA, and SEPM Hamiltonians include spin-orbit interactions. The original data in Ref. 36 did not include spin-orbit interactions. The data listed here in the *GW* column have been corrected from the original data by adding the effects of spin-orbit interactions estimated from our calculations. Unless otherwise stated, the assumed structure is wurtzite and the energies are measured from the top of the valence band $\Gamma_{6v}(A)$. ZB and RS denote the zinc blende and rocksalt structures, respectively. “6.8+*G*” is defined as in Table IV (see caption).

CdSe	LDA	<i>GW</i>	Expt.	SEPM	SLDA	BC
E_{cut} (Ry):	33	25		6.8+ <i>G</i>	6.8+ <i>G</i>	33
$\Gamma_{1,6v}(A)$ [work func.]	-6.29		-5.35 ^a , -6.89 ^b	-5.24	-4.61	
$\Gamma_{1,6v}(A) - \Gamma_{1,6v}(B)$	0.031	-	0.025(±0.002) ^{c,d}	0.027	0.052	-0.076
$\Gamma_{1,6v}(A) - \Gamma_{1,6v}(C)$	0.46		0.43(±0.01) ^{c,d,l}	0.40	0.43	
E_g	0.73	1.78	1.74(±0.1) ^{c,l}	1.72	0.73	1.78
Γ_{3v}	-4.27	-4.57	-5.20(±0.3) ^{e,f}	-4.06	-4.59	-2.53
$\Gamma_{5v}(A+B)$	-0.83	-0.87	-1.20(?) ^e	-0.84	-0.91	-0.58
$\Gamma_{3c} - \Gamma_{5v}(A+B)$	3.11	3.42	4.30(±0.1) ^{g,h,l}	3.96	3.00	4.24
$\Gamma_{6c} - \Gamma_{5v}(A+B)$	6.45	7.25	8.5(±0.15) ^g	7.12	6.26	7.75
Γ_{1v}	-12.19	-12.83	-11.4 ^e	-12.08	-12.27	-14.73
$M_{3c} - M_{4v}$	4.04	5.18	5.2(5.16–5.25) ^{i,h}	4.88	4.07	5.10
M_{1c}	3.39	4.50	4.5(±0.15) ^a	4.17	3.27	4.90
M'_{3c}	4.83	5.86	6.25(±0.15) ^a	5.23	4.71	6.41
M_{4c}	6.35		7.50(±0.15) ^a	6.95	6.24	7.73
M_{4v}	-0.74	-0.85	-1.20 ⁿ	-0.81	-0.90	-0.55
M_{3v}	-1.39	-1.48	-1.70 ⁿ	-1.35	-1.59	-0.70
M_{2v}	-1.74	-1.91	-2.45 ⁿ	-1.79	-1.98	-1.17
M_{1v}	-2.55	-2.79	-3.20 ⁿ	-2.51	-2.87	-1.51
M'_{3v}	-3.65	-3.82	-3.60 ⁿ	-3.37	-3.94	-2.36
M'_{1v}	-4.19	-4.40	-4.90 ⁿ	-3.88	-4.50	-2.70
$H_{3c} - H_{3v}$	4.88		5.75(5.5–6.0) ^{j,g}	5.66	4.93	5.93
$K_{2c} - K_{3v}$	6.05		7.45(7.3–7.6) ^{j,g}	6.34	5.99	7.04
$m_c(\parallel)$	0.07		0.13(±0.01) ^{k,d}	0.13	0.07	0.18
$m_c(\perp)$	0.08		0.13(±0.03) ^{k,d}	0.16	0.08	0.17
$m_{vA}(\parallel)$	1.64		1.30(≥ 1 or 1.2 ± 0.3) ^{d,p}	1.83	1.26	
$m_{vA}(\perp)$	0.18		0.36(0.45 or 0.27 ± 0.1) ^{d,p}	0.29	0.15	
$m_{vB}(\perp)$	0.20		0.9(?) ^d	0.44	0.21	
E_g (ZB)	0.70	1.87	1.68 ^m	1.59	0.59	
$X_{1c} - \Sigma_{4v}$ (RS)	-0.62	0.73	0.70(0.63–0.76) ^{m,o}	0.69	-0.80	
$X_{1c} - L_{3v}$ (RS)	-0.60	0.89	0.70(0.63–0.76) ^{m,o}	0.76	-0.82	

^aReference 22.

^bReference 23.

^cReference 37.

^dReference 38.

^eReference 39.

^fReference 58.

^gReference 40.

^hReference 41.

ⁱReference 42.

^jReference 43.

^kReference 44.

^lReference 45.

^mReference 46.

ⁿReference 47.

^oReference 48.

^pReference 49.

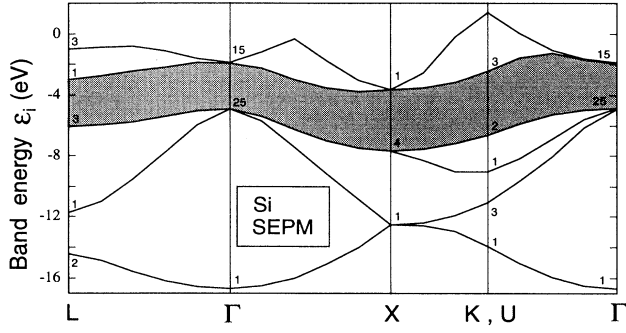


FIG. 8. SEPM band structure of Si in the diamond structure. The spin-orbit interaction is not included. The plane wave cutoff energy is 5.6 Ry. A Gaussian compensating s potential is used. The zero of the energy is the vacuum level.

imental data⁶⁰ for the peak positions. However, in the $E \sim 14$ eV region, the experimental $\epsilon_2(E)$ has larger values than the SEPM results. This too is because we have neglected the Cd $4d$ states in our CdSe SEPM calcula-

tions. The $4d$ electrons have a contribution to $\epsilon_2(E)$ right in the 14 eV region.⁶¹ (iii) The static dielectric constants ϵ_s using $\epsilon_2(E)$ in Figs. 9(b) and 9(c), Fig. 10(b), and Eq. (18) are reported in Table X. For CdSe, the experimental value of ϵ_s is 6.2,^{62,45} while our SEPM result is 5.5. The difference of 0.7 is likely due to the neglect of $4d$ states as explained in Ref. 63.

For Si, the SEPM $\epsilon_2(E)$ misses the first peak apparent in the experimental result.⁶⁴ This peak comes from a large excitonic effect of the Si system,⁶⁵ and thus cannot be described by our single-electron representation (the same is true for all other single-electron methods including the LDA and traditional EPM). The experimental static dielectric constant ϵ_s for Si is 11.4,⁶⁶ while our SEPM result is 10.95 (Table X), slightly larger than the value 10.33 found with the Chelikowsky-Cohen nonlocal empirical pseudopotential. In the light of the large excitonic effect mentioned above and the neglected local field effects, we think the agreement between our result and the experimental result is rather good.

One interesting fact is that, for the LDA, SLDA,

TABLE XII. Comparison for Si of band energies (in eV), band gap E_g (in eV), and effective masses (in units of electron mass) as obtained in the LDA, the LDA with spherically symmetric local potential (SLDA), the semiempirical SEPM, and the traditional empirical pseudopotential method (EPM) (Ref. 35). See Fig. 8 for the identity of the various band state notations used in this table. The energies are measured from the top of the valence band $\Gamma_{25'v}$. No spin-orbit interaction is taken into account. $m_{\Gamma-X}^{(i)}(h)$ and $m_{\Gamma-L}^{(i)}(h)$ stand for the non-spin-coupled effective hole mass [defined as $(\hbar k)^2/2\Delta E$] in the Γ - X and Γ - L directions, where i denotes the band degeneracy. The numbers in the parentheses indicate the experimental uncertainty in the last digit. “5.6+ G ” is defined as in Table IV (see caption).

Si	LDA	Expt.	SEPM	SLDA	CC
E_{cut} (Ry):	20		5.6+ G	5.6+ G	20
$\Gamma_{25'v}$ [work func.]	-5.2	-4.9 ^h	-4.90	-4.74	-
Γ_{1v}	-11.92	-12.5(6) ^e	-11.79	-11.98	-12.36
Γ_{15c}	2.55	3.35(1) ^a	3.01	2.70	3.42
Γ_{2c}	3.14	4.15(5) ^b	4.12	3.75	4.16
X_{4v}	-2.83	-2.9 ^b	-2.78	-2.93	-2.88
X_{1c}	0.62	1.13 ^a	1.26	0.76	1.14
L_{2v}	-9.58	-9.3(4) ^e	-9.52	-9.64	-9.90
L_{1v}	-6.96	-6.8(2) ^e	-6.83	-7.06	-7.10
L_{3v}	-1.17	-1.2(2) ^e	-1.18	-1.25	-1.23
L_{1c}	1.47	2.04(6) ^c	1.96	1.58	2.34
L_{3c}	3.30	3.9(1) ^b	3.88	3.52	4.34
E_{gap}	0.51	1.124 ^d	1.114	0.630	1.009
Σ_{min}	-4.42	-4.48 ^b	-4.26	-4.55	-4.47
$m_L(e)$	0.97	0.92 ^f	0.93	0.92	0.88
$m_T(e)$	0.19	0.19 ^f	0.21	0.19	0.19
$m_{\Gamma-X}^{(2)}(h)$	0.26	0.34 ^g	0.31	0.27	0.31
$m_{\Gamma-X}^{(1)}(h)$	0.17	0.15 ^g	0.19	0.18	0.20
$m_{\Gamma-L}^{(2)}(h)$	0.54	0.69 ^g	0.64	0.59	0.74
$m_{\Gamma-L}^{(1)}(h)$	0.11	0.11 ^g	0.15	0.13	0.12

^aFrom Ref. 50.

^bFrom Ref. 51.

^cFrom Ref. 52.

^dFrom Ref. 53.

^eFrom Ref. 59.

^fFrom Ref. 54.

^gFrom Ref. 55.

^hFrom Ref. 24.

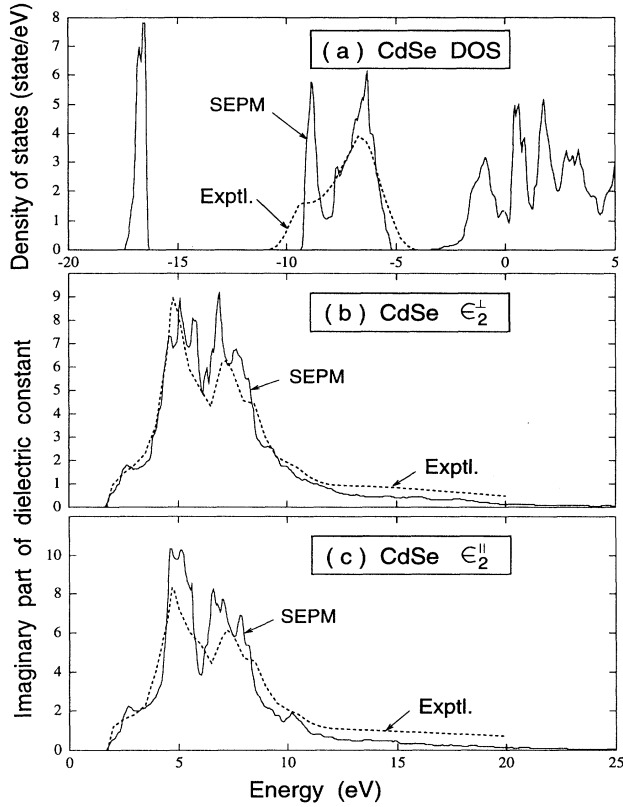


FIG. 9. Density of states (DOS) and imaginary part of dielectric constant (ϵ_2) of CdSe in the wurtzite structure. The solid lines are SEPM results using a plane wave basis set cutoff of 6.8 Ry and a Gaussian compensating s potential. The spin-orbit interaction is included. \perp and \parallel denote perpendicular and parallel to the c axis of the wurtzite structure, respectively. The experimental curve for the DOS is from Ref. 58. The experimental curves for ϵ_2 are from Ref. 60.

and SEPM, the ϵ_s value drops by more than 1 when $\hat{p} + \partial \bar{V}_{\text{nonlocal}} / \partial k$ is used in M_{if} of Eqs. (17) and (18) instead of \hat{p} . But this drop for the Chelikowsky-Cohen nonlocal empirical pseudopotential is only 0.25. This implies that the nonlocal potential of the Chelikowsky-Cohen EPM is very different from the LDA nonlocal potential. This can be confirmed by inspecting the Chelikowsky-Cohen nonlocal potential $v_s(r) - v_p(r)$ (which is roughly a positive 0.55 Ry high spherical step function with a 1 Å radius³⁵) and the LDA nonlocal potential $v_s(r) - v_p(r)$ (which has a maximum high of 6 Ry at $r = 0$, a cutoff radius of 1 Å, and changes from positive to negative values when r crosses 0.6 Å).

IV. CONCLUSIONS

This is not the first work which uses the bulk LDA screened potentials to generate effective atomic potentials (like our SLDA) for various uses. One example is the work of Stokbro *et al.*⁶⁷ These authors used the

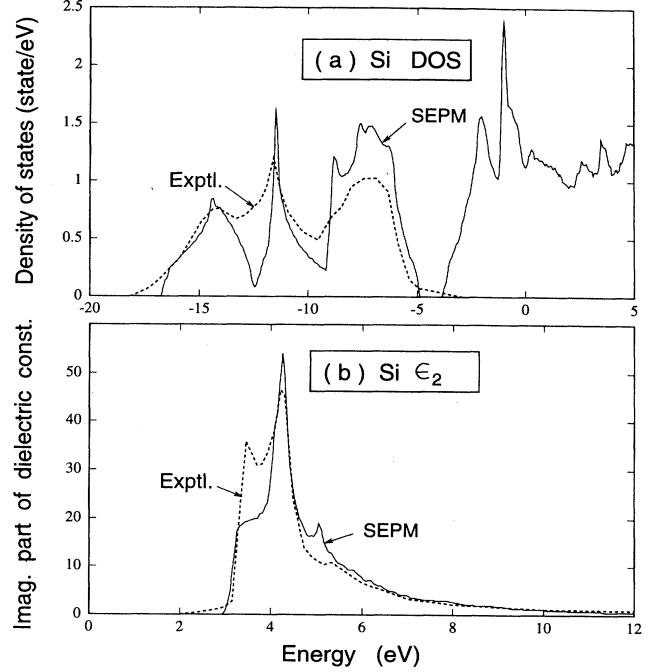


FIG. 10. Density of states (DOS) and imaginary part of dielectric constant (ϵ_2) of Si in the diamond structure. Solid lines are SEPM results using a plane wave basis set cutoff of 5.6 Ry and a Gaussian compensating s potential. The spin-orbit interaction is not included. The experimental curves for the DOS and ϵ_2 are from Ref. 59 and Ref. 64, respectively.

LDA bulk potential to generate a spherically symmetric atomic potential for total energy calculations. In order to apply to dramatically different situations (e.g., surfaces), their spherical potential depends on the local charge density. In contrast, we use here a fixed potential for different crystal structures. This is possible because we only study the bulk systems. Another possible reason for the good transferability of our SLDA potential is that we only study the band structure, not the total energy, thus the results may be less sensitive to the potentials (e.g., 0.1 eV error is considered tolerable).

Our procedure of fitting empirically from SLDA to SEPM is analogous to the *ab initio* GW correction of the LDA results.⁶⁸ Although, conceptionally, the quasiparticle GW approach is different from the LDA approach, in practice one can consider the GW Hamiltonian as a correction to the LDA Hamiltonian for its eigenenergies by adding a self-energy term. Thus both the GW approach and our SEPM approach change the LDA potential, such that the ensuing band energies agree with the experimental results. Our SEPM wave functions have larger than 99.9% overlap with the LDA wave functions. This provides some insights on a long standing puzzle: As reported by Hybertsen *et al.*⁶⁸ the GW single-particle wave function has also larger than 99.9% overlaps with the LDA wave function and this has never been understood. Since in both modifications of the LDA (GW

and SEPM), the ensuing wave functions have $\geq 99.9\%$ overlaps with the original LDA wave function, the reason for this must be rather general, and not a unique property of the GW correction. The reason might be that the original LDA band energies are close enough to the experimental results so that small Hamiltonian modifications ΔH are enough to correct them by first order perturbation $\Delta\epsilon_i = \langle \psi_i | \Delta H | \psi_i \rangle$ without changing the wave functions.

The change from SLDA to SEPM [$u_{\text{SEPM}}^{(\alpha)} - u_{\text{SLDA}}^{(\alpha)}$] (Figs. 4 and 5), although always small, is dependent on the detailed choices of the weights w_i and $\omega_{n,\alpha}$ in Eq. (16). This nonuniqueness is a manifestation of the empirical nature of the fitting. A more *ab initio* approach, using the SLDA and some approximated form of GW self-energy,⁶⁹ might overcome this problem.

Our semiempirical pseudopotential is designed for bulk systems. It can be applied to the most common structures that exist for that material. It can be applied to different volumes for each structure and to the phononic mode of that structure. It remains to be seen whether it can be used in alloy systems, where the type of neighboring atoms for a given atom can change. It could be that some environment dependent scheme, like the linear interpolation method used in Mader and Zunger's approach,⁷⁰ is necessary. The current potential cannot be used in cases where large charge transfer exists, so probably it cannot be used for surfaces.

In summary, we presented an approach to generate semiempirical pseudopotentials. Comparing to the traditional EPM approach, the current method has the following features. (i) A spherically and structurally averaged screened LDA potential, SLDA, is generated. This potential can be used to reproduce the LDA band energies (within 0.1 eV) and wave functions (with overlap $> 99.99\%$) for the most common bulk structures of that material. (ii) The SEPM is fitted from the SLDA. Because the change is very small, many physical trends of the SEPM follow the results of the SLDA (thus LDA) without explicit fitting. Following the transferability of the SLDA, the SEPM can be used for different bulk structures, volumes, and phononic modes. (iii) Because the change from SLDA to SEPM is small, the SEPM wave functions have about 99.9% overlaps with LDA wave functions. (iv) The fitted band structures, density

of states, optical absorption spectra, and static dielectric constants are as good as or better than traditional EPM results compared to experiment. (v) The fitting from SLDA to SEPM is a linear process; thus it is easy and straightforward and guarantees generation of reliable SEPM's.

ACKNOWLEDGMENT

This work was supported by the office of Energy Research, Materials Science Division, U.S. Department of Energy, under Grant No. DE-AC02-83CH10093.

APPENDIX A: SMOOTH PLANE WAVE BASIS CUTOFF METHOD

In a plane wave basis calculation, plane wave functions $e^{i\mathbf{G}\cdot\mathbf{r}}$ are used in the basis set if

$$E(\mathbf{G}, \mathbf{k}) \equiv \frac{1}{2}|\mathbf{G} - \mathbf{k}|^2 \leq E_{\text{cut}}, \quad (\text{A1})$$

where \mathbf{k} is the k point wave vector in the first Brillouin zone and E_{cut} is a cutoff energy which determines the size of the basis set. If E_{cut} is small, the eigenstates (and eigenenergies) of the system are not converged with regard to the basis set. Thus adding or deleting one plane wave function in the basis set will change the results. This causes discontinuities in the band structure because when \mathbf{k} changes a little some plane wave functions may be added in or deleted from the basis set according to Eq. (A1). This phenomenon also manifests itself in calculations for large systems when only the $\mathbf{k} = \mathbf{0}$ states are examined. This is because the $\mathbf{k} = \mathbf{0}$ states of the large system may derived from off- Γ point states in the bulk by k point folding. [In one calculation for a long (~ 100 layers) quantum well, we found that the envelope function of the lowest eigenstate is erroneously $\propto \sin(2\pi x/L)$ instead of the correct one $\propto \sin(\pi x/L)$, where L is the quantum well length.] To smear out this discontinuity, we have used the following smooth cutoff scheme. Still, we use all the plane wave functions of Eq. (A1) as our basis set. Then we define a weight function

$$w(\mathbf{G}) = \begin{cases} 1 & \text{if } E(\mathbf{G}, \mathbf{k}) \leq \beta E_{\text{cut}} \\ \sin^2 \left[\frac{\pi[E_{\text{cut}} - E(\mathbf{G}, \mathbf{k})]}{2(1-\beta)E_{\text{cut}}} \right] & \text{if } \beta E_{\text{cut}} \leq E(\mathbf{G}, \mathbf{k}) \leq E_{\text{cut}}, \end{cases} \quad (\text{A2})$$

where $\beta \leq 1$ is a control factor ($\beta = 0.8$ is used in the current calculations). Then in the G space representation of the Hamiltonian $\hat{H} = \frac{1}{2}(\mathbf{G} - \mathbf{k})^2 + V_{\mathbf{k}}(\mathbf{G}_1, \mathbf{G}_2)$, \hat{H} is changed to $\hat{H}' = \frac{1}{2}(\mathbf{G} - \mathbf{k})^2 + w(\mathbf{G}_1)V_{\mathbf{k}}(\mathbf{G}_1, \mathbf{G}_2)w(\mathbf{G}_2)$. In other words, before the wave function ψ is multiplied by the potential of the Hamiltonian, it is multiplied by $w(\mathbf{G})$ in G space. Computationally, this will add no apprecia-

ble cost. Now when a new plane wave function enters the basis set by Eq. (A1), its $w(\mathbf{G})$ is close to zero. As a result, this plane wave function provides no new variational degree of freedom to lower the potential energy [but it costs kinetic energy $\frac{1}{2}(\mathbf{G} - \mathbf{k})^2$]; hence its variational coefficient is zero and the band structure will not suffer a sudden change. This smooths out the discontinuity in

the band structure (in the long quantum well calculation mentioned above, the erroneous lowest eigenstate disappears). One minor inconvenience of this approach exists: when a constant potential V_0 is added to the original potential \hat{V} of \hat{H} , using this cutoff method, the resulting \hat{H}' is not simply subjected to a constant shift in energy. In our calculation we fix the original potential \hat{V} by requiring the vacuum level to be zero. Another smooth cutoff method which avoids this inconvenience is to change \hat{H} to $\frac{1}{2}(\mathbf{G} - \mathbf{k})^2 w^{-1}(G) + V_{\mathbf{k}}(\mathbf{G}_1, \mathbf{G}_2)$ (for conjugate gradient calculations, the divergence of the kinetic energy term does not pose problems since a proper preconditioner can be used). However, this method increases the total width of the energy spectrum of the Hamiltonian, which makes it difficult to calculate the density of states of large systems when the moments method is used.⁵ As a result, this approach is not used in our study. Finally, when $\beta = 1$, the current smooth cutoff method changes back to the conventional simple cutoff method.

APPENDIX B: SMALL BOX IMPLEMENTATION OF NONLOCAL PSEUDOPOTENTIAL

For large system calculations we need the operation $\hat{H}\psi$ to scale linearly with the size of the system. If the potential \hat{V} in \hat{H} is nonlocal, the traditional G space matrix multiplication method $\sum_{\mathbf{G}'} V(\mathbf{G}, \mathbf{G}')\psi(\mathbf{G}')$ scales as N^2 , where N is the size of the system. Using the Kleinman-Bylander (KB) nonlocal pseudopotential²⁷ is faster than using the traditional method, but it still scales as N^2 , unless the truncated real space implementation is used.²⁸ Here we will introduce a simple, “small box” implementation of the nonlocal pseudopotential based on the traditional method (so that no KB reference wave functions are needed and there is no danger of spurious eigenstates).²⁹ For the traditional angular-momentum-dependent nonlocal pseudopotential, the nonlocal part can be written as

$$\begin{aligned} \hat{V}_{\text{nonlocal}}(\mathbf{r}) &= \sum_{\mathbf{R}_i} \hat{v}_{\text{nonlocal}}(\mathbf{r} - \mathbf{R}_i) \\ &= \sum_{\mathbf{R}_i} \sum_{l,m} |P_{lm}(\mathbf{R}_i)\rangle v_l(|\mathbf{r} - \mathbf{R}_i|) \langle P_{lm}(\mathbf{R}_i)|, \end{aligned} \quad (\text{B1})$$

where \mathbf{R}_i are the atomic positions. Here $\langle P_{lm}(\mathbf{R}_i)|$ is a projection function of angular momentum $\{lm\}$ centered at \mathbf{R}_i and $v_l(r)$ is the l th angular momentum pseudopotential, assumed zero if $r \geq r_{\text{cut}}$, and r_{cut} is about 1 Å. When ψ is applied to $\hat{v}_{\text{nonlocal}}(\mathbf{r} - \mathbf{R}_i)$, only the part of ψ inside $|\mathbf{r} - \mathbf{R}_i| \leq r_{\text{cut}}$ has contributions. This leads us to the following implementation. For a given atom located at \mathbf{R}_i , on the real space numerical grid, consider a small box (denoted by Q) surrounding \mathbf{R}_i with its center grid point closest to \mathbf{R}_i . Define $\psi_Q(\mathbf{r}) \equiv \psi(\mathbf{r})$ for grid points \mathbf{r} inside Q . Then treat $\psi_Q(\mathbf{r})$ as if it were periodic within box Q , and apply it to $\hat{v}_{\text{nonlocal}}(\mathbf{r} - \mathbf{R}_i)$, as in a small supercell calculation. This permits us to first fast Fourier transform $\psi_Q(\mathbf{r})$ to $\psi_Q(\mathbf{G}_Q)$, where \mathbf{G}_Q is the reciprocal lattice vector of the small box Q . We also transform

$\hat{v}_{\text{nonlocal}}(\mathbf{r} - \mathbf{R}_i)$ into \mathbf{G}_Q space as $v_Q(\mathbf{G}_Q, \mathbf{G}'_Q)$. We then calculate

$$\phi_Q(\mathbf{G}_Q) = \sum_{\mathbf{G}'_Q} v_Q(\mathbf{G}_Q, \mathbf{G}'_Q) \psi_Q(\mathbf{G}'_Q), \quad (\text{B2})$$

and fast Fourier transform $\phi_Q(\mathbf{G}_Q)$ back to real space $\phi_Q(\mathbf{r})$ and then add this patch of wave function $\phi_Q(\mathbf{r})$ to the whole space wave function $\hat{H}\psi$. Repeating this process for all the atoms, we complete the nonlocal potential application for the whole system. The computational effort for each atom is fixed (independent of the total size of the system); the whole operation scales linearly to the number of atoms and thus the size of the system.

One approximation is that we treat $\psi_Q(\mathbf{r})$ as if it were periodic in small box Q . To reduce the error of this approximation, we have multiplied $\psi_Q(\mathbf{r})$ by a mask function $f(|\mathbf{r} - \mathbf{R}_i|)$ before it is Fourier transformed into \mathbf{G}_Q space [to insure the Hermiticity of the operation, $f(|\mathbf{r} - \mathbf{R}_i|)$ has also been multiplied to $\phi_Q(\mathbf{r})$]. This mask function is zero (or small in practice) on the boundary of the small box Q , so that $f(|\mathbf{r} - \mathbf{R}_i|)\psi_Q(\mathbf{r})$ is periodic. To compensate the effect of $f(|\mathbf{r} - \mathbf{R}_i|)$ on the nonlocal potential, $v_l(r)f^{-2}(r)$ instead of $v_l(r)$ is used to find $v_Q(\mathbf{G}_Q, \mathbf{G}'_Q)$ in Eq. (B2).

The biggest approximation in this method is the finite size of the small box. In principle, if we have an infinitely fine real space grid, this method will be exact provided the small box covers the nonzero region of the nonlocal pseudopotential. In reality, we have a finite real space grid, so this method introduces small errors which depend on the size of the small box. In our ~ 5 Ry low E_{cut} calculations with numerical Fourier grids roughly twice the size of the basis set sphere in \mathbf{G} space, we find that when the box size is about 1.5 of $2r_{\text{cut}}$ the eigenenergy error is about 0.1 eV, which is tolerable for our calculations.

The most time consuming step in this method is to carry out Eq. (B2). If E_{cut} is large, the number of \mathbf{G}_Q is large and this method becomes slow. However, for our ~ 5 Ry E_{cut} calculation, using a small box size of $\sim 3r_{\text{cut}}$, the number of \mathbf{G}_Q is about 80, so the computation count for each atom is about 80^2 , which is small. We find that the computation time on the nonlocal part is about 1.5–2 times that of all other parts.

The $v_Q(\mathbf{G}_Q, \mathbf{G}'_Q)$ in Eq. (B2) can be calculated once and for all for all the atoms of the same type. The atoms may be at different positions inside their small boxes. This can be treated by applying a phase factor on $\psi_Q(\mathbf{G}_Q)$, thus the same $V_Q(\mathbf{G}_Q, \mathbf{G}'_Q)$ can be used for them. When the spin-orbit interaction is used in the Hamiltonian, the same procedure can be used, except that the dimensions of the $\psi_Q(\mathbf{G}_Q)$ and the matrix $v_Q(\mathbf{G}_Q, \mathbf{G}'_Q)$ will double because of the spin degree of freedom.³⁰ Finally, when the size of the small box is the same as the original supercell, the result of the current method is the same as the traditional G space matrix multiplication method.

- ¹ P. Hohenberg and W. Kohn, Phys. Rev. **136**, B864 (1964).
- ² W. Kohn and L.J. Sham, Phys. Rev. **140**, A1133 (1965).
- ³ D.R. Hamann, M. Schluter, and C. Chiang, Phys. Rev. Lett. **43**, 1494 (1979).
- ⁴ L.W. Wang and A. Zunger, J. Chem. Phys. **100**, 2394 (1994); J. Phys. Chem. **98**, 2158 (1994).
- ⁵ L.W. Wang, Phys. Rev. B **49**, 10 154 (1994).
- ⁶ L.W. Wang and A. Zunger, Phys. Rev. Lett. **73**, 1039 (1994).
- ⁷ L.W. Wang and A. Zunger, Comput. Mater. Sci. **2**, 326 (1994).
- ⁸ D. Brust, J.C. Phillips, and F. Bassani, Phys. Rev. Lett. **9**, 94 (1962); D. Brust, M.L. Cohen, and J.C. Phillips, *ibid.* **9**, 389 (1962).
- ⁹ M.L. Cohen and T.K. Bergstresser, Phys. Rev. **141**, 789 (1966).
- ¹⁰ M.L. Cohen and J.R. Chelikowsky, *Electronic Structure and Optical Properties of Semiconductors* (Springer-Verlag, Berlin, 1989).
- ¹¹ Y.W. Yang and P. Coppens, Solid State Commun. **15**, 1555 (1974).
- ¹² N. Trouillier and J.L. Martins, Phys. Rev. B **43**, 1993 (1991).
- ¹³ F. Bassani and G. Pastori Parravicini, *Electronic States and Optical Transitions in Solids* (Pergamon Press, Oxford, 1975).
- ¹⁴ J. Harris, Phys. Rev. B **31**, 1770 (1985); W.M.C. Foulkes and R. Haydock, *ibid.* **39**, 12 520 (1989).
- ¹⁵ One can evaluate $M_{n,\alpha}^i$ using $C_{\text{SLDA}}^{(\alpha)}(n)$ [i.e., $u_{\text{SLDA}}^{(\alpha)}(q)$]. Then the minimization procedure of Eq. (16) can be iterated for a few times as follows: Let ΔC_{now} be the current ΔC obtained from minimizing Eq. (16). Then using the new coefficients $C_{\text{SLDA}} + \Delta C_{\text{now}}$ one can calculate P_i^{now} . Then using $P_i^{\text{now}} - \sum_{n,\alpha} M_{n,\alpha}^i \Delta C_{\text{new}}^{(\alpha)}(n)$ to replace $P_i^{\text{SLDA}} - \sum_{n,\alpha} M_{n,\alpha}^i \Delta C^{(\alpha)}(n)$ and $[\Delta C_{\text{new}} + \Delta C_{\text{now}}]^2$ to replace the ΔC^2 in Eq. (16), one can minimize F to solve ΔC_{new} . Finally, the ΔC_{now} is updated as $\Delta C_{\text{now}} + \Delta C_{\text{new}}$. Two to three such iterations are enough to get a converged ΔC . Note that $M_{n,\alpha}^i$ needs only be evaluated once; thus the fitting procedure is easy and fast.
- ¹⁶ M.L. Cohen and V. Heine, Solid State Phys. **24**, 38 (1970).
- ¹⁷ S.H. Wei and A. Zunger, Phys. Rev. B **37**, 8958 (1988).
- ¹⁸ S.G. Louie, S. Froyen, and M.L. Cohen, Phys. Rev. B **26**, 1738 (1982).
- ¹⁹ D.M. Ceperley and B.J. Alder, Phys. Rev. Lett. **45**, 566 (1980); J. Perdew and A. Zunger, Phys. Rev. B **23**, 5075 (1981).
- ²⁰ A.N. Mariano and E.P. Warekois, Science **142**, 672 (1963); C.J.M. Rooymans, Phys. Lett. **4**, 186 (1963).
- ²¹ M.T. Yin and M.L. Cohen, Phys. Rev. B **26**, 5668 (1982).
- ²² K.O. Magnusson, U.O. Karlsson, D. Straub, S.A. Flodstrom, and F.J. Himpsel, Phys. Rev. B **36**, 6566 (1987).
- ²³ R.K. Swank, Phys. Rev. **153**, 844 (1966).
- ²⁴ F.G. Allen, J. Phys. Chem. Solids **8**, 119 (1959).
- ²⁵ J.S. Kasper and S.M. Richards, Acta Crystallogr. **17**, 752 (1964).
- ²⁶ S. Baroni and R. Resta, Phys. Rev. B **33**, 7017 (1986); M.S. Hybertsen and S.G. Louie, *ibid.* **35**, 5585 (1986).
- ²⁷ L. Kleinman and D.M. Bylander, Phys. Rev. Lett. **48**, 1425 (1982).
- ²⁸ R.D. King-Smith, M.C. Payne, and J.S. Lin, Phys. Rev. B **44**, 13 063 (1991).
- ²⁹ X. Gonze, P. Kackell, and M. Scheffler, Phys. Rev. B **41**, 12 264 (1990).
- ³⁰ L. Kleinman, Phys. Rev. B **21**, 2630 (1980).
- ³¹ Using a low E_{cut} and a Gaussian correction, the SLDA reproduces very well the wave function overlaps (Table VIII), the momentum matrix elements (Table IX), the optical absorption spectrum ϵ_2 , and the static dielectric constant ϵ_s (Table X) given by the SLDA with a high E_{cut} . Regarding the transition matrix elements, we note that, because of the additional Gaussian s potential and the smooth cutoff operation, we have two additional terms in $\partial \hat{H} / \partial k = \hat{p} + \partial \hat{V}_{\text{nonlocal}} / \partial k + \partial \hat{G} / \partial k + \partial \hat{W} / \partial k$. Here, \hat{G} stands for the Gaussian s potential and \hat{W} stands for the smooth cutoff operation. (Note that the cutoff operation \hat{W} always exists even for a traditional cutoff method. The difference is only that our cutoff is smooth while the traditional cutoff is abrupt.) In Table X, we have listed the results including successive terms in the matrix element M_{if} of Eq. (17). From the data in the table we see that the $\partial \hat{G} / \partial k$ and $\partial \hat{W} / \partial k$ terms do have rather small contributions to ϵ_s .
- ³² For CdSe wurtzite, one additional variable θ is used as a fitting parameter to control the crystal splitting quantity. θ is used to define $E'(\mathbf{G}, \mathbf{k}) = \frac{1}{2}[(G_x - k_x)^2 + (G_y - k_y)^2 + (G_z - k_z)^2 \theta^2]$ which replaces $E(\mathbf{G}, \mathbf{k})$ in the smooth cutoff procedure of Appendix A for the wurtzite structure. While the use of θ is not crucial, it does help to make the fitting better. The resulting θ for CdSe SEPM is 1.13.
- ³³ ftp to ftp.nrel.gov as "anonymous," then change directory to pub/sst/archive/LDA.SEPM, and download all the files in that directory.
- ³⁴ T.K. Bergstresser and M.L. Cohen, Phys. Rev. **164**, 1069 (1967).
- ³⁵ J.R. Chelikowsky and M.L. Cohen, Phys. Rev. B **10**, 5095 (1974).
- ³⁶ O. Zakharov, A. Rubio, X. Blase, M.L. Cohen, and S.G. Louie, Phys. Rev. B **50**, 10 780 (1994); O. Zakharov, A. Rubio, and M.L. Cohen (unpublished).
- ³⁷ V.V. Sobolev, V.I. Donetskina, and E.F. Zagainov, Fiz. Tekh. Poluprovodn. **12**, 1089 (1978) [Sov. Phys. Semicond. **12**, 646 (1978)].
- ³⁸ R.G. Wheeler and J.O. Dimmock, Phys. Rev. **125**, 1805 (1962).
- ³⁹ N.J. Shevchik, J. Tejada, M. Cardona, and D.W. Langer, Phys. Status Solidi B **59**, 87 (1973).
- ⁴⁰ M. Cardona and G. Harbeke, Phys. Rev. **137**, A1467 (1965).
- ⁴¹ I.A. Iliev, M.N. Iliev, and H. Lange, Phys. Status Solidi B **69**, 157 (1975).
- ⁴² R. Ludeke and W. Paul, in *Proceedings of the 7th International Conference on II-VI Semiconducting Compounds, Providence, 1967*, edited by D.G. Thomas (W.A. Benjamin Inc., New York, 1967), p. 123.
- ⁴³ C.R. Fraime and R.L. Heingehold, Bull. Am. Phys. Soc. **12**, 321 (1967).
- ⁴⁴ K.J. Button and B. Lax, Bull. Am. Phys. Soc. **15**, 365 (1970); V.V. Volkov, L.V. Volkova, and P.S. Kireev, Fiz. Tekh. Poluprovodn. **7**, 685 (1973) [Sov. Phys. Semicond. **7**, 478 (1973)]; S. Kubo and M. Onuki, J. Phys. Soc. Jpn. **20**, 1280 (1965).
- ⁴⁵ S. Logothetidis, M. Cardona, P. Lautenschlager, and M. Garrigen, Phys. Rev. B **34**, 2458 (1986).
- ⁴⁶ A.L. Edwards and H.G. Drickamer, Phys. Rev. **122**, 1149 (1961).

- ⁴⁷ K.O. Magnusson and S.A. Flodstrom, *Phys. Rev. B* **38**, 1285 (1988).
- ⁴⁸ A. Onodera, *Rev. Phys. Chem. Jpn.* **39**, 65 (1969).
- ⁴⁹ V.A. Kiselev, B.S. Razbirin, and I.N. Uraltsev, *Pis'ma Zh. Eksp. Teor. Fiz.* **18**, 504 (1973) [*JETP Lett.* **18**, 296 (1973)]; H. Hatano, Y. Kokubun, H. Watanabe, and M. Wada, *Jpn. J. Appl. Phys.* **17**, 1127 (1978); C. Hermann and P.Y. Yu, *Phys. Rev. B* **21**, 3675 (1980).
- ⁵⁰ M. Welkowsky and R. Braunstein, *Phys. Rev. B* **5**, 497 (1972).
- ⁵¹ W.E. Spicer and R.C. Enden, in *Proceedings of the Ninth International Conference of the Physics of Semiconductors*, edited by S.M. Ryvkin (Nauka, Moscow, 1968), Vol. 1, p. 65.
- ⁵² R. Hulthen and N.G. Nilsson, *Solid State Commun.* **18**, 1341 (1976).
- ⁵³ W. Bludau, A. Onton, and W. Heinke, *J. Appl. Phys.* **45**, 1846 (1974).
- ⁵⁴ J.C. Hensel, H. Hasegawa, and M. Nakayama, *Phys. Rev.* **138**, A225 (1965).
- ⁵⁵ G. Dresselhaus, A.F. Kip, and C. Kittel, *Phys. Rev.* **98**, 368 (1955).
- ⁵⁶ B. Batlogg, A. Jayaraman, J.E. Van Cleve, and R.G. Maines, *Phys. Rev. B* **27**, 3920 (1983); A.P. Alivisatos (private communication).
- ⁵⁷ R.J. Elliott, *Phys. Rev.* **96**, 280 (1954).
- ⁵⁸ L. Ley, R.A. Pollak, F.R. McFeely, S.P. Kowalczyk, and D.A. Shirley, *Phys. Rev. B* **9**, 600 (1974).
- ⁵⁹ L. Ley, S.P. Kowalczyk, R.A. Pollak, and D.A. Shirley, *Phys. Rev. Lett.* **29**, 1088 (1972).
- ⁶⁰ J.L. Freeouf, *Phys. Rev. B* **7**, 3810 (1973).
- ⁶¹ R.L. Hengehold and F.L. Redrotti, *Phys. Rev. B* **6**, 2262 (1972).
- ⁶² H.W. Verleur and A.S. Barker, Jr., *Phys. Rev.* **155**, 750 (1967); R. Geick and C.H. Perry, *J. Appl. Phys.* **37**, 1994 (1966).
- ⁶³ Estimated from the difference between experimental $\epsilon_2(E)$ and the SEPM $\epsilon_2(E)$ at $E \sim 14$ eV, the contribution of 4d electrons to ϵ_s is on the order of 0.7. Another way to estimate this contribution is to use Penn's model [D.R. Penn, *Phys. Rev.* **128**, 2093 (1962)]: $\Delta\epsilon_s(4d) = 4\pi N_{4d}/m\Omega_0^{\text{CdSe}} E_{4d}^2$; here, N_{4d} is the number of 4d electrons and E_{4d} is the effective 4d electron transition energy. To get a contribution of 0.7, E_{4d} needs to be 17 eV, which is reasonable.
- ⁶⁴ D.E. Aspnes and A.A. Studna, *Phys. Rev. B* **27**, 985 (1983); G.E. Jellison, Jr. and F.A. Modine, *ibid.* **27**, 7466 (1983).
- ⁶⁵ W.R. Hanke and L.J. Sham, *Phys. Rev. Lett.* **33**, 582 (1974).
- ⁶⁶ R.A. Faulkner, *Phys. Rev.* **184**, 713 (1969); H.W. Icenogle, B.C. Platt, and W.L. Wolfe, *Appl. Opt.* **15**, 2348 (1976).
- ⁶⁷ K. Stokbro, N. Chetty, K.W. Jacobsen, and J.K. Norskov, *J. Phys. Condens. Matter* **6**, 5415 (1994).
- ⁶⁸ M.S. Hybertsen and S. G. Louie, *Phys. Rev. B* **34**, 5390 (1986); see also Z.H. Levine and D.C. Allan, *Phys. Rev. Lett.* **63**, 1719 (1989).
- ⁶⁹ R.W. Godby, M. Schluter, and L.J. Sham, *Phys. Rev. B* **36**, 6497 (1994).
- ⁷⁰ K.A. Mader and A. Zunger, *Phys. Rev. B* **50**, 17393 (1994).